17

Microgravity Processing and Photonic Applications of Organic and Polymeric Materials

Donald O. Frazier, Benjamin G. Penn, David D. Smith, and William K. Witherow
NASA Marshall Space Flight Center
Huntsville, Alabama

Mark S. Paley and Hossin A. Abdeldayem
Universities Space Research Association
NASA Marshall Space Flight Center
Huntsville, Alabama

I. INTRODUCTION

In recent years, a great deal of interest has been directed toward the use of organic materials in the development of high-efficiency optoelectronic and photonic devices. There is a myriad of possibilities among organics which allow flexibility in the design of unique structures with a variety of functional groups. The use of nonlinear optical (NLO) organic materials such as thin-film waveguides allows full exploitation of their desirable qualities by permitting long interaction lengths and large susceptibilities allowing modest power input [1]. There are several methods in use to prepare thin films, such as Langmuir–Blodgett (LB) and self-assembly techniques [2–4], vapor deposition [5–7], growth from sheared solution or melt [8,9], and melt growth between glass plates [10]. Organics have many features that make them desirable for use in optical devices such as high second- and third-order nonlinearities, flexibility of molecular design, and damage resistance to optical radiation. However, their use in devices has been hindered by processing difficulties for crystals and thin films.

In this chapter, we discuss photonic and optoelectronic applications of a few organic materials and the potential role of microgravity on processing these materials. It is of interest to note how materials with second- and third-order nonlinear optical behavior may be improved in a diffusion-limited environment and ways in which convection may be detrimental to these materials. We focus our discussion

on third-order materials for all-optical switching, and second-order materials for frequency conversion and electrooptics.

A. Third-Order Materials for Optical Switching

Optical-fiber communication systems have undergone stunning growth over the past decade. The technologies that have arisen in support of these systems have been incredibly fortuitous. The operating wavelength of erbium-doped amplifiers, for instance, serendipitously coincides with the minimum loss wavelength of fused silica fibers. But, even as fiber-optic networks have been implemented on a universal scale, electronic switching is still the main routing method. Although fibers have dramatically increased node-to-node network speeds, electronic switching will limit network speeds to about 50 Gb/s. Already, it is apparent that terabit-rate speeds will soon be needed to accommodate the 10–15%/month growth rate of the Internet and the increasing demand for bandwidth-intensive data such as digital video [11].

All-optical switching using nonlinear optical materials can relieve the escalating problem of bandwidth limitations imposed by electronics. Several important limitations need to be overcome, such as the need for high $\chi^{(3)}$ materials with fast response and minimum absorption (both linear and nonlinear), development of compact laser sources, and reduction of the switching energy. The goal of minimizing optical loss obviously depends on processing methods. For solution-based processes, such as solution crystal growth, electrodeposition, and solution photopolymerization, it is well known that thermal and solutal density gradients can initiate buoyancy-driven convection. Resultant fluid flows can affect transport of material to and from growth interfaces and become manifest in the morphology and homogeneity of the growing film or crystal. Likewise, buoyancy-driven convection can hinder production of defect-free, high-quality crystals or films during crystal and film growth by vapor deposition.

The guided-wave materials used most commonly have been inorganic fibers and semiconductors. Less developed but highly promising are organic materials such as conjugated polymers which possess large nonlinearity, with fast response times, are more easily tailored at a molecular level and more malleable than their inorganic counterparts. One of the major challenges for proponents of organic materials is to find cheap, reliable methods of waveguide fabrication that takes advantage of existing technologies. Processing techniques and choices of materials should result in a minimization of both scattering and absorption losses. One of the main reasons that organic and polymeric materials are not more strongly competitive with silica fibers for switching applications is due to the maturity of silica fiber processing.

B. Second-Order Materials for Electrooptic Applications

Applications of materials with second-order nonlinearity include frequency conversion, high-density data storage, and electrooptic modulators and switches. The first demonstration of second-harmonic generation was in quartz [12] and it has traditionally been observed in inorganic crystals. A decade later it was demonstrated that the second-order nonlinearity may be several orders of magnitude larger in organic crystals possessing delocalized π-electron systems in which intramolec-

ular charge transfer occurs between electron donor and acceptor substituents [13]. Although organic materials may offer larger nonlinearities than inorganic crystals, the utilization of organic crystals is limited by the small number of molecules with large hyperpolarizabilities that have a noncentrosymmetric crystalline state (11 of the 32 crystal classes possess inversion symmetry and cannot be used as $\chi^{(2)}$ materials). Also, the maturity of inorganic crystal growth is relatively advanced, whereas that of organic crystal growth has not had the necessary time for comparable development.

Whereas the second-order nonlinearity in inorganic systems is a bulk effect ascribable to crystalline structure, the primary contribution to bulk nonlinearity for organic systems is due to the ensemble of nonlinearly responding molecules. Van der Waals forces between mers (molecular units) are small and the induced dipoles result most directly from the external field. This provides an added degree of flexibility for organic materials because the required asymmetry does not require crystalline structure but, instead, may be achieved in amorphous geometries. For example, instead of relying on the art of crystal growth, electric field poling of polymers containing the nonlinear chromophore may be used to induce macroscopic asymmetry. Alternatively, self-assembly or liquid-crystal ordering can achieve required asymmetry, possibly encouraged in environmental quiescence such as that offered by reduced convection during microgravity processing.

In order to take advantage of the large nonlinearities in organic materials resulting from π-electron mobility while also utilizing the mechanical and thermal properties of inorganic crystals, some researchers have turned to a semiorganic approach in which organic molecules are bound to an inorganic host by complexation or salt formation. For example, semiorganic single crystals of L-histidine tetrafluoroborate (HFB) have demonstrated five times the effective second-order nonlinearity of potassium dihydrogen phosphate (KDP) [14]. Single crystals are easily obtained from solution and crystals are thermally stable with a decomposition temperature of 205°C. Solution crystal growth has been performed repeatedly in microgravity, particularly for the study of protein crystal growth. Many organics, also good NLO materials, are amenable to solution growth and are ideal candidates for studies of the kinetics and fluid dynamics of solution growth processes. Knowledge of such processes can lead to significant improvement in crystals grown in space or on Earth. Several research tasks are underway to study the growth of bulk single crystals of important materials, such as HFB, L-arginine phosphate (LAP), and several other organic and semiorganic molecules. There is certainly evidence that gravity could play a role in the growth of macromolecular crystals (e.g., protein crystals) as well as on solution polymerization processes. Rosenberger et al. studied the temperature dependence of protein solubility and applications to crystallization and growth kinetics. Within these studies, they observed relative interfacial kinetics and bulk transport as functions of supersaturation and resultant effects on the growth morphology of lysozyme and horse serum albumin [15]. Supersaturations driven by thermal fluctuations on the order of 1–2°C during growth lead to significant optical and structural nonuniformity in a growing crystal. Pusey et al., using tetragonal lysozyme, showed that forced fluid flow rates of 30–40 μm/s slow and eventually stop the growth of 10-μm crystals [16,17]. Cessation of growth occurred at flow rates as low as 2.5 μm/s in some crystals, but growth persisted over a longer period of time than at higher fluid flow rates. The conclusion is that for

some crystals at least, even small convective flows are deleterious for growth of the crystal. The precise mechanism for this is not yet understood, but, clearly, the case is quite strong for studying the growth of certain organic and semiorganic crystals in microgravity environments.

It is therefore reasonable to consider that microgravity can play an important role in the formation of organic and semiorganic crystals for second-order applications. In the diffusion-limited regime of space, larger and more defect-free crystals may be grown, hence improving optical transparency and conversion efficiency. By different processing techniques, improved optical quality and molecular alignment have been observed in polydiacetylene (PDA) and phthalocyanine (Pc) thin films processed in microgravity or reduced convection environments. Perhaps of more immediate relevance, knowledge gained from low-gravity (low-**g**) experiments may enable the optimization of growth conditions on Earth.

C. Material Limitations

1. Dispersion and Loss

One limitation governing the propagation of pulses in a waveguide is the reshaping of the pulse due to group velocity dispersion (GVD). Each frequency component in the pulse sees a different refractive index and thus travels at a different speed through the medium, leading to a spreading or reshaping of the pulse. GVD is more important for short pulses, as they contain more frequency components. This pulse spreading reduces the amount of information that can be carried and destroys the cascadability (the ability of the output of a device to reenter an identical device and behave similarly) of the system. It is quite obvious that losses due to film imperfections must contribute significantly to this limitation, and processing methods must strive to ensure minimization of material defects. However, a pulse also consists of different intensities. Each intensity can also see a different refractive index due to the nonlinearity of the medium and so travels at a different speed. The ability of a pulse to become reshaped due to the nonlinearity of the medium is known as self-phase modulation (SPM). For certain pulse shapes, GVD is exactly balanced by SPM and the pulse retains its shape over an infinite propagation distance in the absence of loss. GVD pulses that are balanced by SPM are known as solitons. In practice, however, solitons cannot propagate infinitely. The effect of dissipation decreases the peak power in the pulse, hence decreasing SPM. The result is that the soliton widens as it propagates. Two main sources of loss are operative in silica fibers: an intrinsic loss due to Rayleigh scattering and, superimposed on this, absorption due to hydroxide ion impurities in the melt [18]. Due to the maturity of silica fiber fabrication technology, impurities in the melt can be kept quite low. Microgravity processing may enable polymeric materials to become more competitive with silica fibers by the reduction of similar types of scattering loss mechanisms.

2. Two-Photon Absorption

A major setback to the development of an all-optical switch is the existence of nonlinear loss manifested by multiphoton absorption. The current strategy is to search for a truly nonresonant operating wavelength. To demonstrate the deleterious effects of multiphoton absorption, consider its effect on a simple device. A nonlin-

ear directional coupler (NLDC) is a device in which two waveguides or fibers are brought close together such that their overlapping evanescent attenuations periodically transfer power back and forth between the guides as light propagates through the device [19]. The periodicity of phase-matched power transfer depends on channel separation and refractive index. Full power transfer occurs after one coupling length, L_c. When the length of the overlapping region equals the coupling length, all the power will be transferred to the neighboring guide. If the guide material has a large cubic nonlinearity (and hence nonlinear refractive index n_2), the coupling will be perturbed at high intensities due to an intensity-dependent phase mismatch in the guides, and at the switching power, the majority of the transmission will switch from one guide to the other. The majority of the coupler's output may then be toggled between the guides simply by raising and lowering the intensity.

Multiphoton absorption occurs when the intensity of the radiation causes virtual levels to become accessible. Transition rules prohibit transitions between same-parity states unless virtual levels are involved. Because two-photon absorption (TPA) is intensity dependent, it varies with propagation distance. The result is that the power transfer is accompanied by increasing TPA in the low-intensity guide and decreasing TPA in the high-intensity guide such that complete switching does not occur or is suppressed (Fig. 1). Mizrahi et al. [20] have shown that TPA places a fundamental constraint on the usefulness of any high-$\chi^{(3)}$ material. Semiconductors, for example, are constrained to energies below half the band gap to avoid TPA [21,22].

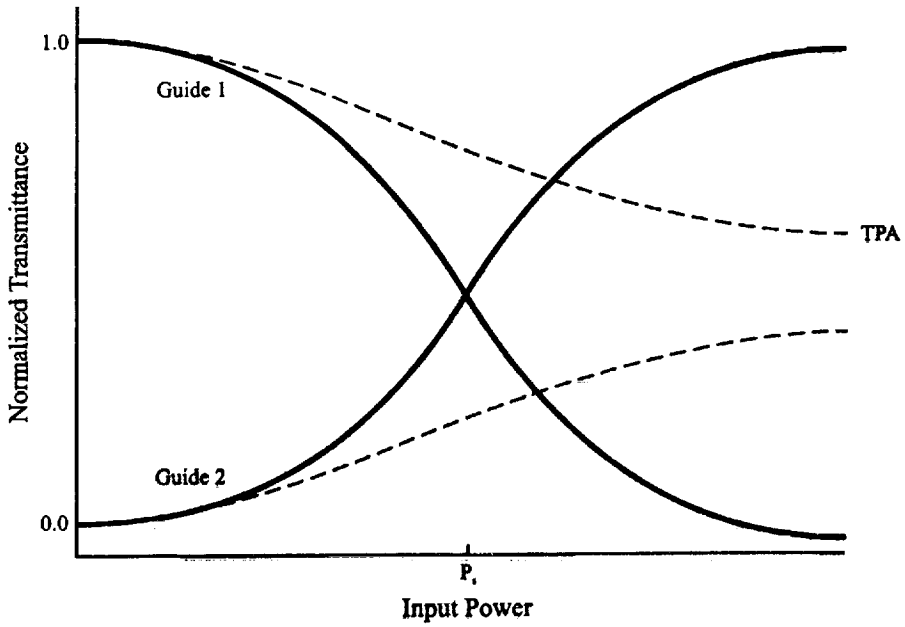

FIGURE 1 Effect of two-photon absorption on a nonlinear directional coupler. The coupler is initially in a crossed state. Increasing input power perturbs the coupling which causes switching, suppressed by the presence of TPA.

An alternative approach based on materials architecture is elimination of induced absorption. Specifically, the nonlinear absorption in a material may be canceled by the addition of small metal particles. This approach is possible because of a counterintuitive consequence of local field effects that was first recognized by Hache et al. [23]. They found that for gold nanoparticles in glass, the colloid as a whole demonstrated saturable absorption. However, the isolated metal behaved quite differently, demonstrating induced absorption. Embedding the particles in a glassy matrix altered the sign of the nonlinear absorption as a result of the local field correction. The implication of Hache's finding is that there is a concentration somewhere between pure gold and the colloidal gold glass at which the imaginary part of the cubic susceptibility goes to zero. In fact, if the sign of Im $\chi^{(3)}$ is the same for each component, then, by necessity, there will actually be two concentrations at which Im $\chi^{(3)}=0$. The smaller concentration crossing point is obviously more useful because it entails a lower amount of linear absorption and poses less of a challenge to fabricate. The significance and specificity of particle concentration demands careful control of metal particle dispersion. This requirement is also prevalent in the crystal growth of certain semiconducting alloys where the optimum band gap is determined by alloy stoichiometry. Lehoczky et al. directionally solidified $Hg_{0.84}Zn_{0.16}Te$ alloy in microgravity with some success at purely diffusion-controlled growth to achieve the desired stoichiometry throughout the space-grown crystal. However, unexpected transverse residual accelerations from the shuttle environment resulted in some radial compositional variations [24]. The result stresses the difficulty in achieving precise concentrations during materials processing where thermal or concentration gradients arise and could be fatally disruptive in terms of achieving a defined concentration objective. Considering difficulties in achieving diffusion-controlled growth and other desirable gravitationally sensitive results during microgravity processing, ground-based attempts at overcoming these effects may prove futile. Where homogeneous dispersion and concentration are requisite in materials of interest, processing on Earth-orbiting platforms could offer distinct advantages.

To demonstrate the cancellation of absorptive nonlinearity of a composite aqueous system, Smith [25] performed open-aperature Z-scan measurements on a gold colloid prepared by the recipe of Turkevich [26] at various particle concentrations. A frequency-doubled ND : YAG laser at 532 nm provided 30-ps mode-locked pulses at a repetition rate of 10 Hz. Each concentration was placed in a 1-cm optical-path-length quartz cuvette on a track near the focus of the beam. The focal length of the lens was 33 cm and the full width at half-maximum (FWHM) beam diameter was 2.5 mm. The beam waist was measured to be $w_0=70$ μm, corresponding to a Rayleigh diffraction length of $z_0=2.9$ cm.

Instead of two-photon absorption, however, the nonlinear mechanism was reverse saturable absorption. The system consisted of a known reverse saturable absorber 1,1′,3,3,3′,3′-hexamethylindotricarbocyanine iodine (HITCI) in methanol and water. The proportions of dye, methanol, and water were held fixed. Because these chemicals form a solution, they may be considered a single component, although their chemical association should be accounted for by a modification of the local field factor as described by Fröhlich [27]. The other component was the gold. The proportions of the various components are illustrated in Table 1. Note that the

TABLE 1 Component Properties of HITCI/Au Composite

CURVE No.	GOLD COLLOID (ml)	WATER (ml)	123 μM HITCI (ml)	METHANOL (ml)
1	0	2.75	0.4	0.6
2	0.5	2.25	0.4	0.6
3	1.0	1.75	0.4	0.6
4	1.5	1.25	0.4	0.6
5	1.9	0.85	0.4	0.6
6	2.0	0.75	0.4	0.6
7	2.2	0.55	0.4	0.6
8	2.5	0.25	0.4	0.6
9	2.75	0	0.4	0.6

same amount of dye, methanol, and water is used in each case and that the only variable is the concentration of gold. The Z-scans for various concentrations of gold are displayed in Fig. 2. It can be clearly seen that the nonlinear absorption changes sign near curve 6. The experiment was repeated several times and the sign reversal was obvious each time. Note that curves 1–5 display a valley indicative of reverse saturable absorption. At the focus, however, a small secondary peak is observed. This peak corresponds to a saturation of the nonlinear absorption and was first reported by Swatton et al., [28]. A four-level semiclassical model was used to describe the absorption of the dye.

D. Candidate Materials

1. *Fused Silica Fibers Versus Conjugated Organics*

Figures of merit have been proposed to describe the linear and nonlinear losses and the dispersion in candidate materials [20,22,25,29–32]. Fused silica fibers are attractive for optical communications systems because, although they have a relatively weak nonlinearity, they have among the highest figures of merit due to their low loss in the region—1.3–1.6 μm, known as the telecommunications window. Also, silica fibers exhibit anomalous (negative) dispersion for wavelengths greater than 1.3 μm, allowing solitons to propagate. The two wavelengths most commonly used for communications are the zero dispersion wavelength of 1.3 μm and the low-loss wavelength of 1.55 μm. The wavelength of choice has become 1.55 μm due to the availability of multiple-clad dispersion-shifted fibers.

A rule of thumb for all-optical switches is that $\chi^{(3)}LI$ (path length and intensity) is constant [11]. So, although silica fibers have a much lower cubic nonlinearity, $\chi^{(3)}$, the switching power can be much lower than that of other materials because there is almost no length limitation on a fiber; whereas, typically for a highly nonlinear material, the loss is much greater, imposing a length limitation. But simply increasing the switch's operating length does not take into account the dispersion or spreading of the pulse, which becomes more important for very short pulses. For fused silica fibers, the dispersion can be tuned negative to support solitons, but most highly nonlinear materials have positive GVD in the telecommunications win-

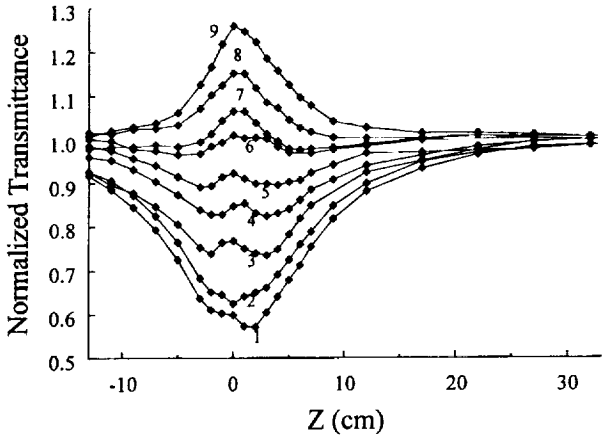

FIGURE 2 Elimination of induced absorption in HITCI by the addition of small Au particles. For each Z-scan, the peak power was P_i = 0.16 MW and the on-axis peak irradiance at focus was I_0 = 2.1 GW/cm^2.

dow and thus cannot support solitons for these wavelengths. One way to decrease the switching energy without the switching power is to use shorter pulses; however, this also increases dispersion. Thus, for long pulses, fibers are not constrained by pulse spreading and can operate at lower powers, but for short pulses, materials with higher nonlinearities may switch at lower powers due to GVD considerations. Asobe et al. have shown that for very short pulses, when group velocity dispersion is taken into account, highly nonlinear conjugated polymers will operate at a lower switching energy than positive dispersion silica fibers [32]. As we will show, microgravity may be exploited to reduce the length limitation in polymeric waveguides.

An additional reason for choosing highly nonlinear conjugated polymers over silica fibers is because of limitations which arise from the propagation design of the device. Switching in silica fibers requires very long lengths of fiber which can seriously reduce the switching time and result in cumbersome setups.

2. Gravitational Effects in Processing Organic and Polymeric Films

Two promising classes of organic compounds for optical thin films and waveguides are polydiacetylenes (PDAs), which are conjugated zigzag polymers, and phthalocyanines, which are large ring-structured porphyrins. Epitaxial growth on ordered organic and inorganic substrates under various processing conditions have been useful for preparing highly oriented polydiacetylene (PDA) and phthalocyanine (Pc) films [33–35]. The degree of significance relating processing conditions to uniformity in thickness, degree of orientation, and optical properties for a specific processing technique is the general focus of work in this area. A study on the effect of processing conditions relevant to thin-film deposition by various techniques is particularly difficult because of the possibility that convection may play a major role. It is a goal of some researchers to produce good quality anisotropic films; therefore, an important yet understudied requirement should be to assess the role of gravity during processing. This may be particularly true for the vapor deposition of diace-

tylenes where subsequent polymerization in the crystal is topochemical and occurs readily only when neighboring monomer molecules are sufficiently close and suitably oriented [29]. Likewise, this requirement is equally viable for the vapor deposition of Pcs in view of the results of microgravity experiments by 3M Corporation involving the preparation of thin films of copper Pc (CuPc) [34–44]. Indeed, a variety of microstructural forms was obtained in thin films of CuPc dependent on processing methods and conditions. Small changes in processing parameters caused large changes in molecular orientation within the film. Microgravity grown CuPc had several desirable features which indicate that the growth of organic films in low **g** may result in better quality films for optical and electrical applications [43,44]. The dramatic 3M result was very encouraging and has been one source of optimism toward considering the microgravity environment of value for processing high-quality organic films.

One goal of microgravity research on vapor-deposited organic films is to understand factors for improving film quality and optical properties. Important aspects of any study involving fluids, as in vapor transport, are driving mechanisms for heat transfer with natural convection and diffusion processes which determine flow profiles and temperature distributions.

A novel technique, recently discovered, for growing polydiacetylene thin films involves exposing a transparent substrate, in contact with diacetylene monomer solution, to ultraviolet (UV) light [45]. A polymer film deposits on the side of the substrate in contact with monomer in solution, and there are distinct gravitational effects which influence film quality. Good quality thin films elude growth from solutions absent of uniform flow fields and homogeneous temperature distributions near the substrate surfaces. The flow fields and temperature distributions during the polymerization process by exposure to UV light details the nature of gravitational influences on this process.

From a device perspective, the UV technique makes construction of extremely complex waveguides possible. Utilizing a computer-controlled x–y translation stage, programmed to trace out a desired pattern, researchers demonstrated that UV radiation (364 nm) from an argon ion laser could trace out a test pattern [46] (Fig. 3a). It is possible to construct a Mach–Zehnder interferometer with an optimized curvature using this technique [47]. After mounting a test cell containing diacetylene monomer solution on a translation table, a focused UV laser beam passing through the UV transparent surface of the test cell traced the desired paths to form the polymer-based optimized Mach–Zehnder waveguide (Fig. 3b).

It has been proposed that NLO thin-film properties may be improved by low-gravity processing using electrodeposition. Strong candidates for NLO thin-film applications are the polythiophenes. Polymeric thiophenes are attractive materials due to their ease of preparation, stability, and high third-order susceptabilities [48–52]. A simple and convenient method for preparation of polythiophenes is electrochemical oxidation. Earlier microgravity experimentation [53,54] on metal,metal/cermet electrodeposition of Ni provides some microgravity electrodeposition background and raises the possibility of application to improving the quality of polythiophene thin films in low gravity. Electrodeposition of Ni on a Au substrate in low gravity often results in the production of an x-ray nondiffracting surface. Similarly deposited cobalt metal does not give this result nor does Ni on a glassy carbon substrate. Further, the Co/Ni alloy composition variance during electrodep-

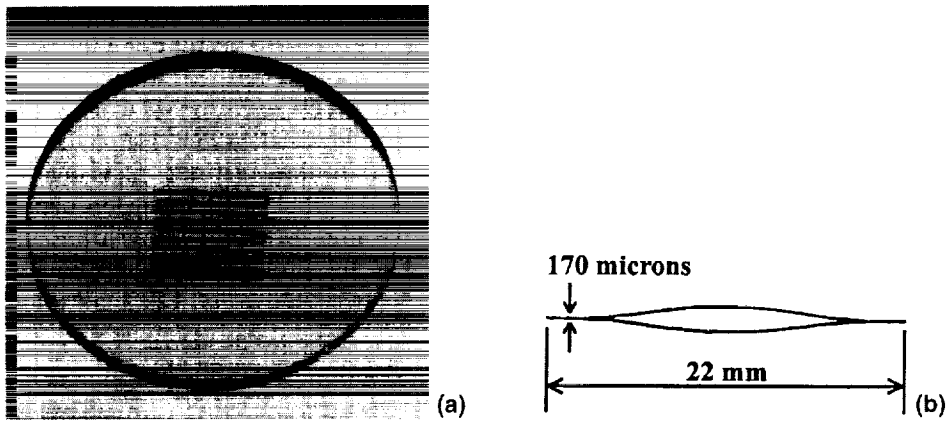

FIGURE 3 A PDA film derived from 2-methyl-4-nitroaniline (MNA) circuit photodeposited onto UV transparent substrates using the radiation from an argon ion laser: (a) demonstration pattern on a quartz disk; (b) enlarged image of an actual Mach–Zehnder interferometer on a glass microscope slide.

osition is strongly dependent on the amount of convection. Similar sensitivities to gravitational influences apparent in inorganics during electrodeposition should arise during electrodeposition of organics.

Electrochemical polymerization deserves thorough investigation for use in fabricating thin-film waveguides. NLO films might be prepared on the surface of various substrates during polymerization for the fabrication of devices. This method has been useful in the synthesis of several polymers, in addition to the polythiophenes, such as polypyrrole and polyazulene. The probable existence of thermal and concentration gradients in such dynamic processes suggest an assessment of gravitational influences on film morphologies is justified.

II. GROWTH OF THIN FILMS BY VAPOR DEPOSITION

A. Phthalocyanine Thin Films

This class of materials is an excellent candidate for use in developing NLO devices because of their two-dimensional planar π-conjugation, better chemical and thermal stability than most other organic materials, and ease of derivatizing through peripheral and axial positions (Fig. 4). Large [55–64] and ultra fast [52,65,66] third-order nonlinearities have been demonstrated for phthalocyanines (Pc). The nature of the central metal atom strongly influences the value of $\chi^{(3)}$. Shirk et al. [56] measured the third-order susceptibility of tetrakis(cumyl phenoxy) phthalocyanines by degenerate four-wave mixing at 1.064 μm. The $\chi^{(3)}_{xxxx}$ values for Pt–Pc (2×10^{-10} esu) and Pb–Pc (2×10^{-11} esu) were found to be approximately 45 and 5 times that of the metal-free phthalocyanine form (4×10^{-12} esu), respectively. Other researchers have shown that $\chi^{(3)}$ of Pc's increase about 15 times by changing the central metal atom from silicon to vanadium [67] and there is also an increase when the central atom is a heavy metal atom such as lead [68]. These positive

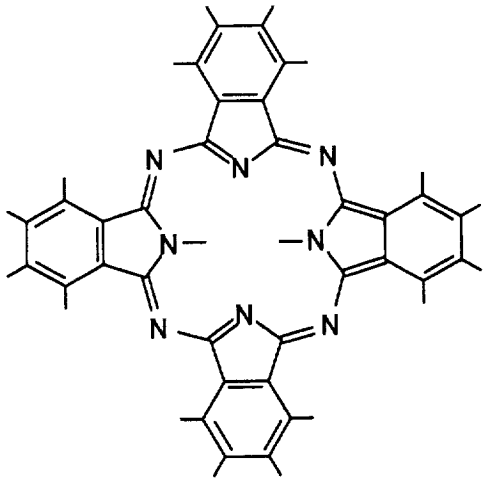

FIGURE 4 Metal-free phthalocyanine (H_2Pc).

influences of metal substitution on the third-order optical nonlinearity are attributed to the introduction of low-lying energy states derived from metal-to-ligand and ligand-to-metal charge transfer [56].

Recently, phthalocyanine-related compounds have emerged as novel candidates for second-order nonlinear optical applications. Sastre et al. [69] measured a β value of 2000×10^{-30} for the trinitro-substituted boron sub-phthalocyanine (SubPc) whose structure is shown in Fig. 5. SubPc's are two-dimensional 14 π-electron-conjugated macrocycles that are composed of three isoindole units containing boron inside. The reported second-order hyperpolarizability for the trinitro derivative is comparable to that of the most efficient linear or dipolar compound.

Difunctional tetraarylporphyrins with nitro groups as electron acceptors and amino groups as electron donors were observed to have a substantial hyperpolarizability by Suslick et al. [70]. The β values for *cis*-diamino–dinitro- and triamino–mononitro-substituted tetraarylporphyrins were 30×10^{-30} esu and 20×10^{-30} esu, respectively. These derivatives were prepared by the partial reduction of the nitro groups of 5, 10, 15, 20-tetrakis-(p-nitrophenyl) porphyrin. Li et al. [71] measured a relatively large second-harmonic generation (SHG: $\chi^{(2)}_{zzz} \sim 2 \times 10^{-8}$ esu) for covalently bound self-assembled monolayer thin films of 5, 10, 15, 20-tetra (4-pyridyl) 21 H, 23 H–porphine and its derivatives on quartz and silicon ⟨100⟩ substrate having a native oxide layer.

Thin films of Pc for fabrication of waveguides can be obtained by physical vapor transport because of their exceptional thermal stability and ease in sublimation. Matsuda et al. [58] observed that Pc with axial ligands (e.g., vanadyl phthalocyanine) have higher $\chi^{(3)}$ values than most usual unsubstituted Pc. The $\chi^{(3)}$ values of thin films of Pc vacuum deposited at 10^{-4} Pa onto fused quartz are shown in Table 2. The maximum values for the unsubstituted Pc's at 1.9 μm were 1.5×10^{-12} esu for CuPc and 0.8×10^{-12} esu for NiPc. In comparison, chloro-indium Pc and vanadyl Pc had $\chi^{(3)}$ values of 1.3×10^{-10} esu and 3×10^{-11} esu, respectively. Ho et al. [55] grew films of chloro-gallium (GaPc–Cl) and fluoro-

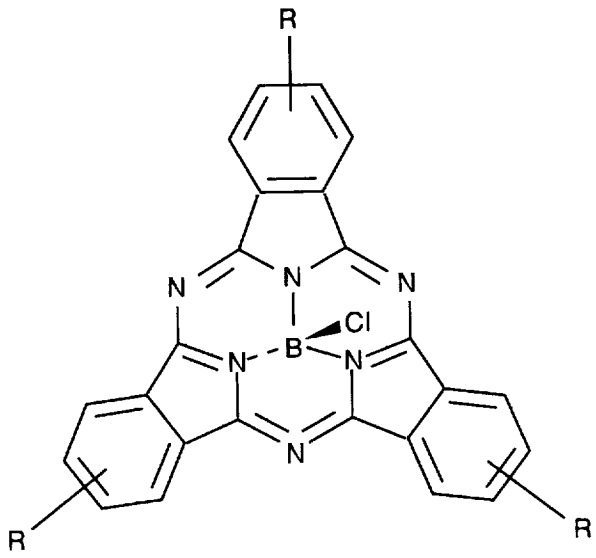

FIGURE 5 Trinitro-substituted boron sub-phthalocyanine (SubPc).

aluminum (AlPc–F) phthalocyanines onto fused silica flats at 150°C and 10^{-6} Torr. The $\chi^{(3)}$ values for GaPc–Cl and AlPc–F were 5×10^{-11} and 2.5×10^{-11} esu at 1064 nm for thickness of 1.2 μm and 0.8 μm, respectively.

Wada, et. al. [72] measured a $\chi^{(3)}$ of 1.85×10^{-10} esu at 1.907 μm for a 51.4-nm-thick film of vanadyl phthalocyanine (VOPc) vacuum deposited onto quartz.

TABLE 2

Compound	Film thickness (μm)	$\chi^3 \times 10^{-12}$ esu (1.9 μm)
Unsubstituted phthalocyanine		
Copper phthalocyanine (CuPc)	0.53	1.5
Cobalt phthalocyanine (CoPc)	0.22	0.76
Nickel phthalocyanine (NiPc)	0.35	0.80
Platinum phthalocyanine (PtPc)	0.41	0.60
Unsubstituted phthalocyanine with axial ligands		
Vanadyl phthalocyanine (VOPc)	0.28	30
Titanyl phthalocyanine (TiOPc)	0.26	27
Chloro-aluminum phthalocyanine (ClAlPc)	0.26	15
Chloro-indium phthalocyanine (ClInPc)	0.14	130

The $\chi^{(3)}$ values for two different phases in vanadyl and titanyl (TiOPc) phthalocyanines were measured by optical third-harmonic generation at wavelengths of 1543 nm and 1907 nm by Hosoda et al. [73]. The transformation of as-prepared Pc's films from phase I to phase II was performed by thermal annealing and was accompanied by a red shift in absorption spectra and an increase in $\chi^{(3)}$ values of two to three times. $\chi^{(3)}$ values for as-prepared films of VOPc and TiOPc were 3.8 $\times$ 10^{-11} esu and 10^{-11} esu, whereas the annealed films had values of 8.1 $\times$ 10^{-11} esu and 4.6 $\times$ 10^{-11} esu, respectively.

Recently, a relatively strong SHG was reported for vacuum-deposited copper phthalocyanine (CuPc) films which possess inversion symmetry. Chollet et al. [74] measured a $d_{\text{eff}} \approx 2 \times 10^{-19}$ esu at 1.064 μm fundamental wavelength for films with thickness ranging from 50 to 500 nm that were prepared at a pressure of 10^{-6} Torr and source temperature of 120°C. The films were homogeneous and partly oriented with a relatively large distribution of molecular axes oriented almost prependicular to the substrate. This order was confirmed by SHG measurements. SHG in the films was attributed to quadrupolar or dipolar origins. Kamagai et al. [75] prepared 40–2000-Å thick films at a pressure of 5 $\times$ 10^{-6} Torr and obtained $\chi^{(2)}_{zyy}$ = 4 $\times$ 10^{-8} esu at a 1.06 μm fundamental wavelength, which is one-fourth the value for $LiNbO_3$. They proposed a mechanism in which an asymmetric crystal field acting perpendicular to the surface makes each CuPc molecule capable of SHG. Yamada et al. [76] performed in situ observation of SHG from CuPc films during vacuum evaporation on glass at a pressure of 1.5 $\times$ 10^{-5} Torr and a rate of 1.2 nm/min. Thickness dependence on SHG was compared with calculations based on electric dipole, electric quadrupole, and magnetic dipole mechanisms to clarify the origin of SH activity. Based on the comparison, SHG was ascribed to electric quadrupolar or, preferably, magnetic dipolar origin.

The research of Debe et al. [77–79] indicates that better quality organic thin films for use in NLO devices might be obtained by closed-cell physical vapor transport (PVT) in microgravity. In the PVT process, the source material is sublimed in an inert gas and allowed to convect or diffuse down a thermal gradient and to ultimately condense at a crystal or thin-film growth interface [77]. The advantage of thin-film growth in microgravity is that it provides the opportunity to eliminate buoyancy-driven convection. Recent reports [77–79] of the Space Shuttle mission STS-51 of August/September 1985 include results of experiments in which CuPc was epitaxially deposited, by PVT, onto highly oriented seed films of metal-free phthalocyanine (H_2Pc). The substrate was a 1.4-cm-diameter solid copper disk.

The PVT of organic solids (PVTOS) apparatus used to grow CuPc thin films consisted of nine identical metal/Pyrex ampoules housed within its own heater assembly and vacuum insulation cell [77,78,80]. Films were grown in 1.7-cm-diameter by 7.5-cm-long Pyrex tubes that were placed within resistance-wire-wound heaters which induced a nonlinear axial thermal gradient. The growth ampoules were filled primarily with CO_2, H_2, the buffer gas Xe, or He, and then either N_2 or CO as the next most abundant component. A computer-controlled heater maintained the hot end of the ampoule, containing the source, at 400°C for 4 h after the cruise temperature was reached. The substrate was maintained at a temperature of 70°C by a heat pipe.

The substrate seed film was prepared by vacuum sublimation of H_2Pc onto a copper disk at a temperature range known to produce highly oriented films. A

metal-free phthalocyanine film with a thickness of 1100 ± 50 was grown at a deposition rate of 70 Å was grown at a deposition rate of 70 Å/min. The substrate was held at a temperature of 5–10°C and the source-to-substrate distance was 16 cm. Debe has shown that highly oriented films of H_2Pc are obtained when the substrate temperature range is approximately 5 ± 5°C [80]. Before starting the growth process, the source material was out-gassed by slowly increasing the temperature of the hot zone. After ~ 2 h of "soaking," the temperature was increased to cause the H_2Pc material to deposit on the copper substrate at a pressure of about 5×10^{-6} Torr.

Microgravity grown CuPc films had several desirable features which indicate that the growth of organic films in low g may result in better quality films for NLO applications. For example, results of analysis by visual photography, bright-field and differential interference contrast microscopy, scanning ellipsometry, visible reflection spectroscopy, and direct interferometric phase-contrast microscopy imply that the Space grown films were radially more uniform and homogeneous, and an order of magnitude smoother over the submillimeter to submicron scale range [77]. Results of analysis involving the use of external reflection–absorption infrared (IR) spectroscopy, grazing incidence x-ray diffraction, and visible–near-IR reflection–absorption spectroscopy infer that the microgravity grown films are more highly uniaxially oriented and the films were found to consist predominantly of crystalline domains of a previously unknown polymorphic form of CuPc [78]. In addition, scanning electron microscopy analysis revealed that there was a distinctly different microstructure in the center of the Space grown films and that the circular perimeters of the microgravity grown films had microstructure much like that of the ground control films in both their center and edge regions [79].

As stated earlier in the chapter, electric field poling of polymers containing the nonlinear chromophore may be used to induce macroscopic asymmetry. However, in the case of the ring-structured macromolecule, phthalocyanine, poling is not generally an option to achieve ordering in deposited films. It is, therefore, beneficial to achieve, if possible, self-assembly to induce required asymmetry by other means. Whenever self-assembly might occur in molecules not prone to poling, exploitation of conditions favorable toward asymmetry could prove beneficial. In the case of Pc, for example, $\chi^{(3)}$ enhancement and possible $\chi^{(2)}$ inducement might result from self-assembly. Vapor-deposited H_2Pc have demonstrated some potentially interesting nonlinear optical properties. Researchers report these films to be randomly oriented when processing occurs in 1 **g** (Fig. 6a) [43,44,77–80]. From microgravity processing, CuPc films epitaxially deposited onto H_2Pc films are highly oriented and densely packed (Fig. 6b). Abdeldayem et al. [81] recently observed intrinsic optical bistability in vapor-deposited thin films of metal-free Pc, ranging in thickness from 40 to 800 nm, using continuous-wave (CW) and chopped He–Ne lasers at 633 nm. Source and substrate temperatures were maintained at 300°C and 5°C, respectively, whereas vapor vacuum deposition occurred at 10^{-6} Torr onto quartz disks. Bistability in the film was attributed to changes in the level of absorption and refractive index caused by thermal excitation. This nonlinear effect could improve dramatically in highly oriented microgravity processed films.

For a discussion of optical bistability, we first recognize that the absorption spectrum in the visible region shows a strong maximum at 626 nm. In one experiment [81], the CW He–Ne (632.8 nm) laser at a fixed input power of ~30 mW

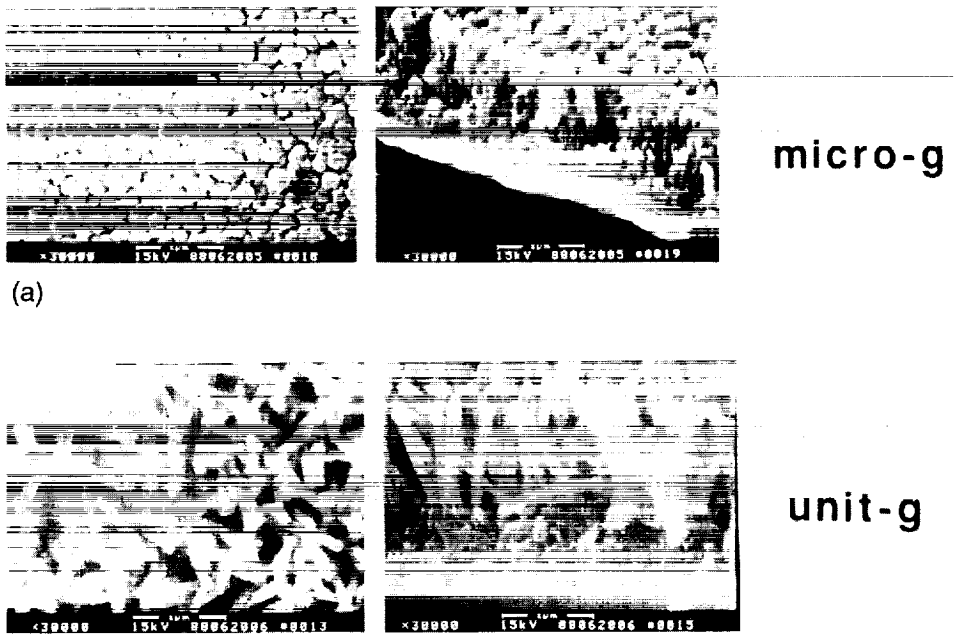

(a)

(b)

FIGURE 6 Copper phthalocyanine films epitaxially vapor deposited onto copper substrate a) μ-**g** deposition of CuPc epilayer; (b) 1-**g** deposition of CuPc epilayer. (Courtesy of 3M Corporation.)

was focused on a 230-nm-thick-film. The beam transmission increased temporally over a period of nearly 12 h, as shown in Fig. 7a. The nearly straight line of Fig. 7b is a fraction of the input power for monitoring laser stability. Fitting the transmission data to a single exponential (the solid line) gave a rise time of ~2.2 h to reach a steady state.

The temporal transmission effect in the film can be explained by the following sequence: (a) The initial low transmission of the beam through the film can be attributed to a strong absorption of the beam which generates free electrons and holes; (b) these free charges relax to excitonic states [82] and release their excess energy as heat to the system at the focal point; (c) the buildup of localized heating at the focus reduces absorption of the He–Ne radiation causing saturation of absorption. This factor is in agreement with the results of a separate experiment to measure the sample's absorption at a temperature elevated above room temperature by a water bath. Such reduction in absorption allows more transmission to occur with time.

Investigation of the bistability of metal-free Pc films of 833 nm thickness used a chopped He–Ne 632.8-nm laser beam at frequencies ranging from 100 to 750 Hz. The film was positioned on a micrometer stage, at the lens focus, and transversely translated in and out of the beam alternately to record intensity input and film transmittance. A Hewlett-Packard (HP) digitizing oscilloscope model 54120B recorded the input and the transmitted pulse with a HP plotter model 7470A (Fig. 8). The nonsymmetrical shape of the transmitted pulses (Fig. 8b) indicated the

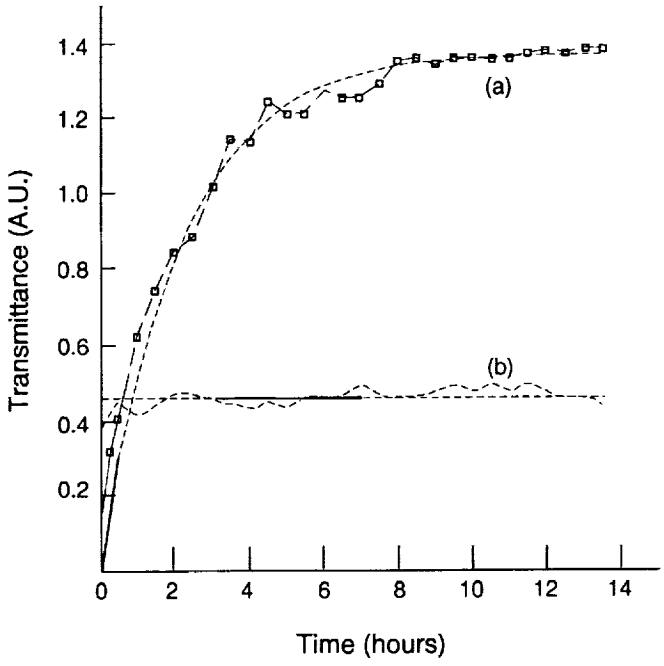

FIGURE 7 (a)Time-dependent transmittance through a metal-free phthalocyanine film (230 nm thick), using a CW He–Ne laser at 632.8 nm and 30 mW power. The dotted curve represents the experimental data, whereas the solid line represents a single exponential theoretical fit. (b) The dotted line represents laser stability throughout the experiment, and the solid line is the corresponding straight-line fit.

presence of intrinsic bistability in metal-free phthalocyanine. Figure 8c depicts typical bistable switching, constructed from the transmitted pulse. The switching power of ~0.33 mW per pulse in combination with a pulse duration of 1.37 ms recovery time yields a very low switching energy of ~0.45 nJ. Observation of bistability was repetitive in the same film using a CW He–Ne laser as shown in Fig. 9 for different time spans between successive points.

A thinner film, 230 nm, also demonstrated saturation of absorption at the same He–Ne laser frequency. Figure 10 illustrates the experimental data recording absorption by a 230-nm-thick film and the theoretical curve fit assuming Bloch-type saturable absorption with negligible scattering losses [83]:

$$a(I)L = \left(\frac{a_0 L}{1 + I/I_s}\right) \tag{1}$$

where I_s is the threshold power of the saturation, L is the thickness of the sample, and a_0 is the linear absorption coefficient. The saturation intensity, estimated from the theoretical fit, is

$$I_s \sim 2.0 \times 10^4 \quad \frac{\text{W}}{\text{cm}^2}$$

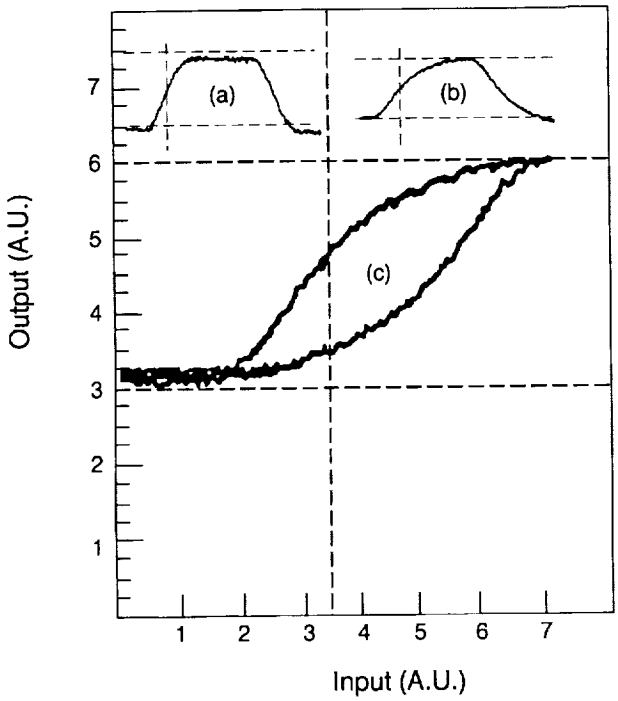

FIGURE 8 The bistability loop of a 833-nm metal-free phthalocyanine film using a chopped CW He–Ne laser at 632.8 nm: (a) the input pulse, (b) the transmitted pulse, (c) hysteresis switching constructed from (b).

Modeling phthalocyanine as a three-level system, a molecule in the ground state at saturation absorbs light at a rate

$$\frac{1}{t} = s_0 I_s / hf \tag{2}$$

where t is the decay time of the excited triplet state, I_s is the saturation intensity, s_0 is the absorption cross section of the ground state, and hf is the energy of the incident photon. From the measurements of the fall time of 1.0756 ms at 245 Hz in Fig. 8b, the absorption cross section was estimated [84] to be on the order of $\sim 2.4 \times 10^{-17}$ cm^2.

The estimated third-order nonlinear susceptibility measurements by four-wave mixing using a pulsed Nd : YAG laser at 532 nm was on the order of 10^{-8} esu. This relatively large value is attributed to both resonant as well as thermal mechanisms that might be present in the system at this wavelength.

B. Polydiacetylene Thin Films

1. *Second- and Third-Order Nonlinear Optical Properties of Polydiacetylenes*

Polydiacetylenes (Fig. 11) are highly conjugated organic polymers that are of considerable interest because of their unique chemical, optical, and electronic prop-

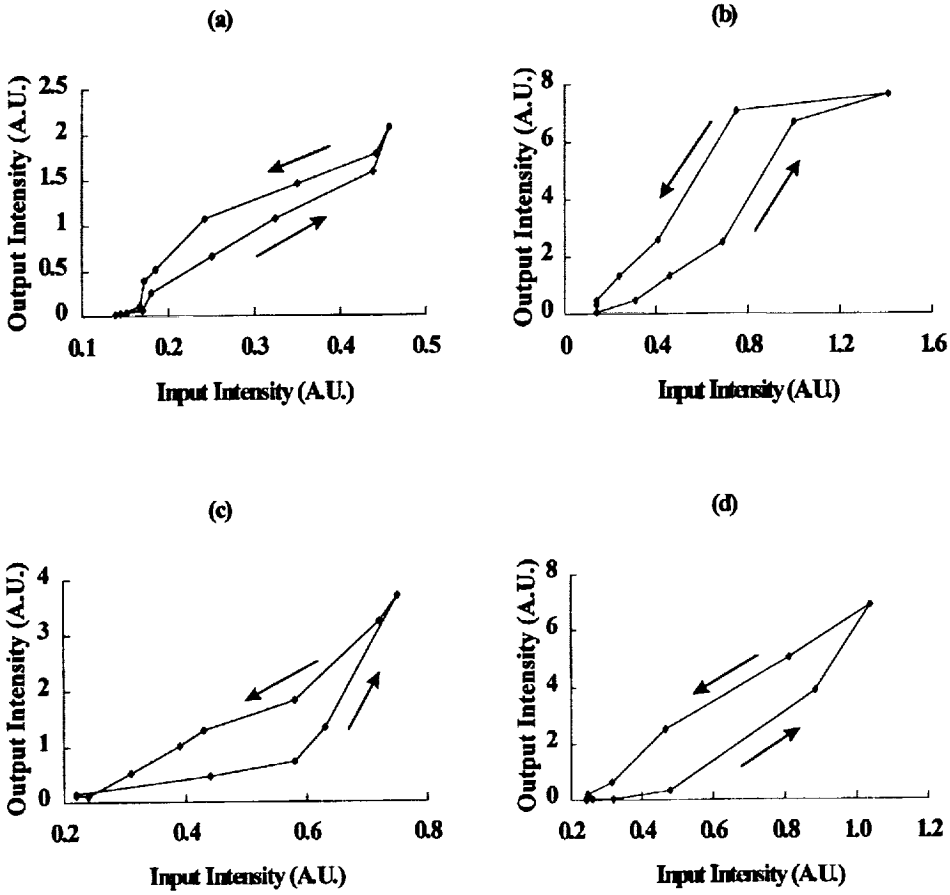

FIGURE 9 The bistability loops for different time spans of a metal-free phthalocyanine film of thickness 232.5 nm using a CW He–Ne laser. Time spans between successive points are (a) 3.84 s, (b) 10 s, (c) 342 s, and (d) 1800s. Part (a) shows the least prominent bistability loop; parts (b), (c), and (d) show a minimal effect of the time span between points.

erties [85–88]. This class of polymers has received extensive attention as organic conductors and semiconductors, as well as NLO materials. The high mobility of the π electrons in the polymer backbone allows them to have large optical/electrical susceptibilities with fast response times; they can be highly ordered, even crystalline, which is important for optimizing their electronic and optical properties, and they can readily be formed into thin films, which is the preferred form for many applications. The physical, chemical, and mechanical properties of polydiacetylenes can be varied by varying the functionality of the side groups, thereby making it possible to tailor their properties to meet specific needs. Thus, there is a great deal of interest in the use of these polymers for technological applications.

Polydiacetylenes are among the best known third-order NLO materials, and there has been considerable investigation over the past 20 years into their properties. Single crystals of poly(2,4-hexadiyne-1,6-ditosylate), also known as PTS, pos-

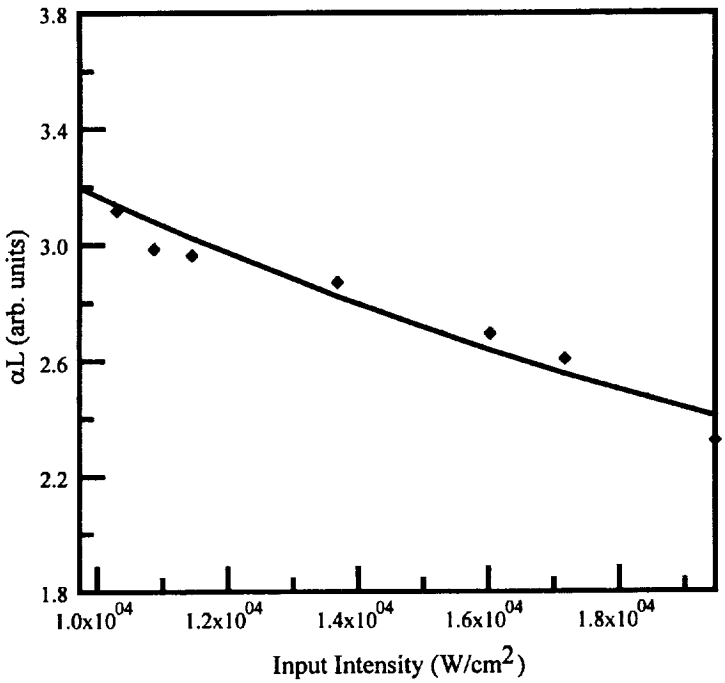

FIGURE 10 Experimental and theoretical fitting of saturable absorption of a metal-free phthalocyanine film (232.5 nm thickness) at 632.8 nm from a CW He–Ne laser. The corresponding saturation intensity is 19.8×10^3 W/cm^3.

sess one of the largest (possibly the largest) nonresonant third-order optical nonlinearities ever measured, on the order of 10^{-9} esu [89]. The third-order NLO properties of numerous other polydiacetylene crystals and thin films have also been determined. Typical $\chi^{(3)}$ values for polydiacetylenes range from 10^{-7} to 10^{-12} esu, depending on the degree of resonance enhancement and other factors. Both theoretical and experimental results have determined that the $\chi^{(3)}$ value is approximately 100 times greater along the polydiacetylene backbone than perpendicular to it, demonstrating the effect of the conjugated π-electron system. Because the origin of the nonlinearity is electronic, they can have very fast response times, on the order of femtoseconds.

More recently, polydiacetylenes have been investigated as potential second-order NLO materials. Theoretical calculations have indicated that certain polydiacetylenes could possess extremely high second-order NLO susceptibilities (e.g.,

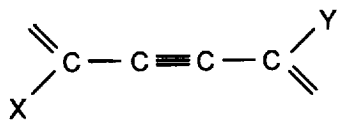

FIGURE 11 Structure of polydiacetylene repeat unit.

molecular hyperpolarizabilities on the order of 10^{-27} esu [90]. In order to make use of this second-order nonlinearity, it is necessary to orient the polymers into acentric structures, either crystals or thin films. This is not trivial; many compounds which have desirable properties at the molecular level tend to orient themselves centrosymetrically in the bulk to minimize electrostatic interactions.

Second-harmonic generation (SHG) has been observed from certain asymmetrical liquid-crystalline diacetylene monomers (although, interestingly, not from the corresponding polymers) [91], from both LB and self-assembled polydiacetylene monolayers and multilayers [92,93] and even from a spin-coated polydiacetylene film [94]. Finally, powder SHG efficiences comparable to that of MNA (2-methyl-4-nitroaniline) have been obtained from vapor-deposited polycrystalline films of a polydiacetylene possesing MNA as a side group [90]. If the crystallites are partially aligned by growing the films quasi-epitaxially onto prealigned poly(tetrafluoroethylene) substrates, the SHG efficiency increases by almost one order of magnitude.

2. Potential Benefits of Microgravity Processing

Optical applications require the formation of high-quality thin polydiacetylene films (i.e., films possessing minimal defects such as impurities, inhomogeneities, light scattering centers, etc.). The standard techniques for obtaining polydiacetylene thin films involve the growth of crystalline diacetylene monomer films or the deposition of LB films, followed by topochemical polymerization of these films in the solid state to yield ordered polydiacetylene films. This ability to undergo solid-state polymerization is a very intriguing property of diacetylenes; in principle, one can start with a single-crystal monomer and obtain a single-crystal polymer [7,95]. However, the process is not trivial; the formation of high quality crystalline diacetylene monomer films or LB films can be very tedious and difficult, and, furthermore, by no means do all monomers polymerize readily in the solid state [8]. Achieving high-quality polydiacetylene films requires the growth of high-quality diacetylene monomer films, which are then topochemically polymerized. A commonly employed technique for obtaining diacetylene monomer films is vapor deposition. One of the chief limitations to vapor deposition of high-quality monomer films (e.g., single-crystalline films with good molecular orientation and few defects) has been a lack of understanding of how the processing conditions affect monomer film growth. It is certainly well known that parameters such as temperature, pressure, concentration, and so forth can affect vapor transport processes. One parameter which is often tacitly ignored is the influence of gravity. However, the effects of gravity, such as buoyancy-driven convection, can greatly influence heat and mass transport during the growth process, and thereby influence all of the aforementioned growth parameters. Thus, discerning the effects of gravity (or the lack thereof) could play a critical role in optimizing the growth of high-quality polydiacetylene films by vapor deposition.

One method of assessing convection in a gas phase is to perform the computation at low pressure to relieve the need for specific materials constants. It is important to note that buoyancy effects are possible only if the molecular mean free path is short enough relative to cell dimensions such that molecular flows are not in the free molecular flow regime. A mathematical model has been developed to determine buoyancy-driven heat transfer in an ideal gas under a variety of ori-

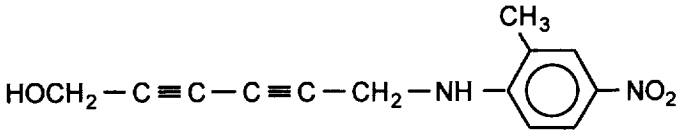

FIGURE 12 Diacetylene monomer (DAMNA).

entations relative to gravitational accelerations [97]. The model demonstrates that convection can occur at total pressures as low as 10^{-2} mm Hg in cells having relatively high length-to-width ratios. A preliminary experimental test of the model involved deposition of the diacetylene monomer, DAMNA (Fig. 12), at an evacuation pressure of 10^{-2} mm Hg.

The deposition of DAMNA by physical vapor transport was of 30 min duration. Cell dimensions were the same as those depicted in Fig. 13 with source temperature of 120°C and sink temperature of 30°C. The evacuation pressure reached a minimum in the presence of DAMNA (10^{-2} mm Hg) and was significantly lower in the absence of DAMNA. It is probable that the DAMNA vapor pressure is equal to, or greater than, the evacuation pressure of 10^{-2} mm-Hg. From a different study, the measured vapor pressure of 4-*N*,*N*-dimethylamino-4′-nitrostilbene (DANS) at 120°C was reportedly 0.374 mm [98]. This is a relatively large organic molecule

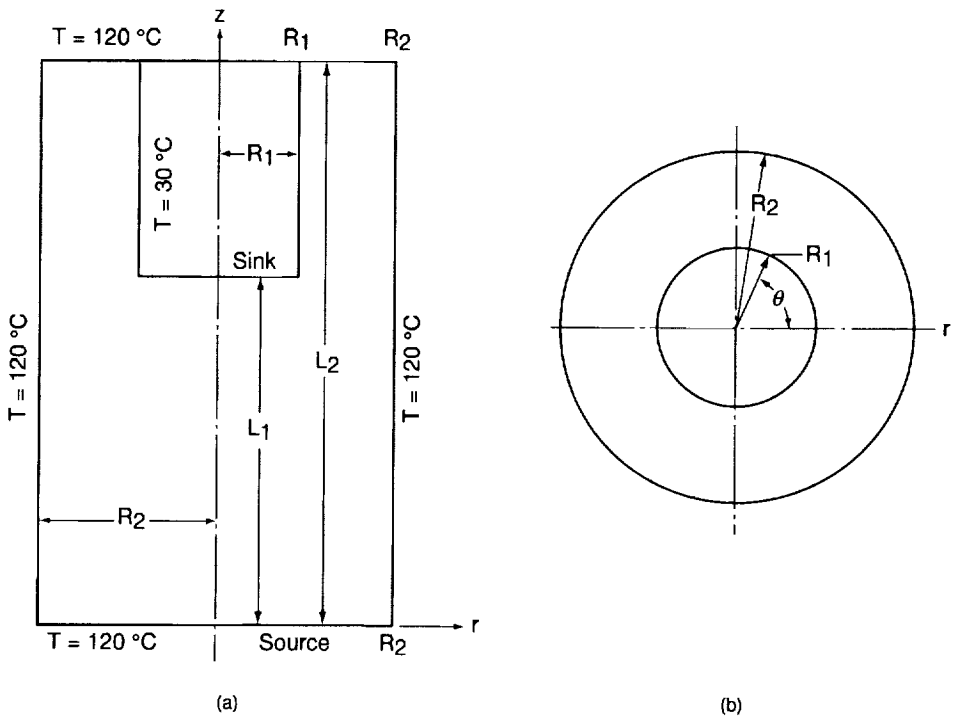

FIGURE 13 Vapor-deposition cell for physical vapor transport of DAMNA.

having a molecular weight of 211 g/mol as compared to DAMNA with a molecular weight of 247 g/mol. Considering structural and size similarities, we may approximate similarities in vapor pressure. Indeed, heptadecanol (molecular weight = 256.5 g/mol), also an alcohol with possible hydrogen bonding in its condensed phases such as expected of DAMNA, has a vapor pressure of 10^{-1} mm at 120°C [99]. There is no reason to expect DAMNA to differ drastically from these measured vapor pressures, and we may approximate that the vessel evacuation pressure minimum is largely due to the vapor pressure of DAMNA.

Using physical material parameters of air, a series of time steps demonstrates the development of flow and temperature profiles in an ideal gas. These profiles are driven by the specified temperatures with no mass fluxes (there are no subliming or condensing masses in this model) in a vessel as specified in Fig. 13. Computations show that in unit gravity, it is possibly that vapor deposition occurs by transport through an axisymmetric circulating flow pattern when applying heat to the bottom of a vertically positioned vessel. In the case where heating of the reaction vessel occurs from the top, deposition of vapor does not normally occur by convection due to a stable stratified medium. When vapor deposition occurs in vessels heated at the bottom, but oriented relative to the gravity vector between these two extremes, horizontal thermal gradients induce a complicated asymmetric flow pattern.

Comparison of Figs. 14 and 15 and Figs. 14 and 16 show the differences in induced flow fields in the θ = 0°–180° and θ = 90°–270° planes, respectively, driven by vertical and tilted cavities. There are two recirculation flows generated with centers at (r_c, z_c) = ($\pm$1.90 cm 2.7 cm) and at (r_c, z_c) = ($\pm$0.8cm, 3.2 cm) for flows induced by vertical and tilted orientations, respectively. For the vertical orientation, the flow depicted in Fig. 14 is axisymmetric, hence also representative of flows in the θ = 90°–270° plane. The flows are upward along the surface of the outer cylinder and downward from the central column. These are Bernard-type flows driven by counterrotating cells (clockwise on the left and counterclockwise on the right) due to an incipient instability in the narrow cylindrical cell cavity. There is no critical Rayleigh number for convection which assumes an infinite extent of the cell width. For the tilted cell, a resultant asymmetric flow in the θ = 0°–180° plane approaches an antisymmetric flow profile resulting from differential heating between vertical and opposite walls of a cavity; that is, an incipient instability causes heat to flow along the bottom surface (now tilted upward), upward along the side wall, along the cold surface (downward), and downward along the other side wall. The two recirculation flows for this orientation appear in the θ = 90°–270° plane (Fig. 16). There is an upward flow from the bottom surface of the outer cylinder transporting heat toward the bottom surface of the central column with downward flows on the outside walls (clockwise on the right and counterclockwise on the left). This asymmetric three-dimensional flow profile is quite complex and represents a greater degree of convection in the cell cavity for the tilted orientation than for the vertical orientation. The model material parameters for air predict the effect of kinematic viscosity to be of the same order as thermal diffusivity, which is the case for Prandtl number (Pr) ~1 fluids [100]. The classical heat capacity for a gaseous molecule, such as DAMNA, with its large number of vibrational degrees of freedom, is only achieved at high temperatures; that is, the heat capacity of DAMNA will approach that of a diatomic molecule, such as the

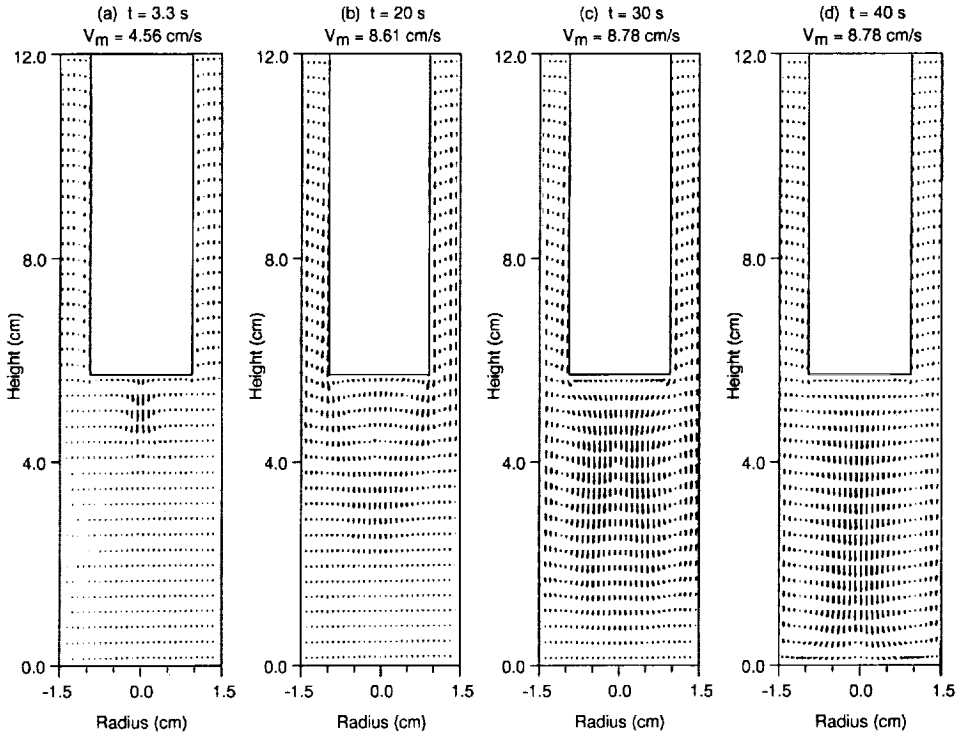

FIGURE 14 Axisymmetric flow in the $\theta = 0°–180°$ plane in a cell in which deposition occurs with cell oriented vertically.

major components of air, because its vibrational modes are unable to store energy at these relatively low temperatures. The thermal diffusivity approximation using air data is, therefore, a fair one, assuming similar heat conduction coefficients. In the classical limit, the higher heat capacity would yield Pr >> 1. Because an ideal heat capacity approximation is an overestimate at the operating temperatures, deviation from ideal behavior causes Pr ~ 1, closer to that of air. Without actual data for DAMNA, we are left with experimental data from the low operating pressures and temperatures to compare with modeling estimates. Close agreement between experiment and the model would indicate that DAMNA at these pressures indeed approximates an ideal gas with the appropriate deviations which tend toward validation of the use of air physical constants. Furthermore, the constant heat flux provided by the circulating bath is a factor in neutralizing thermal effects specific to individual molecules.

Experimentally, it is helpful to utilize Beer–Lambert's relationship for transmission of radiation through a medium to test gravitationally sensitive flow pattern predictions [97]. We would expect that the flow patterns in Figs. 15 and 16 (cell tilted at 45° relative to gravity vector) would affect film quality over most of the deposition surface differently than the flow pattern depicted in Fig. 14 (cell oriented vertically). Preliminary experiment suggests this to be the case with respect to film thickness. The Beer–Lambert law relative to film thickness can be written

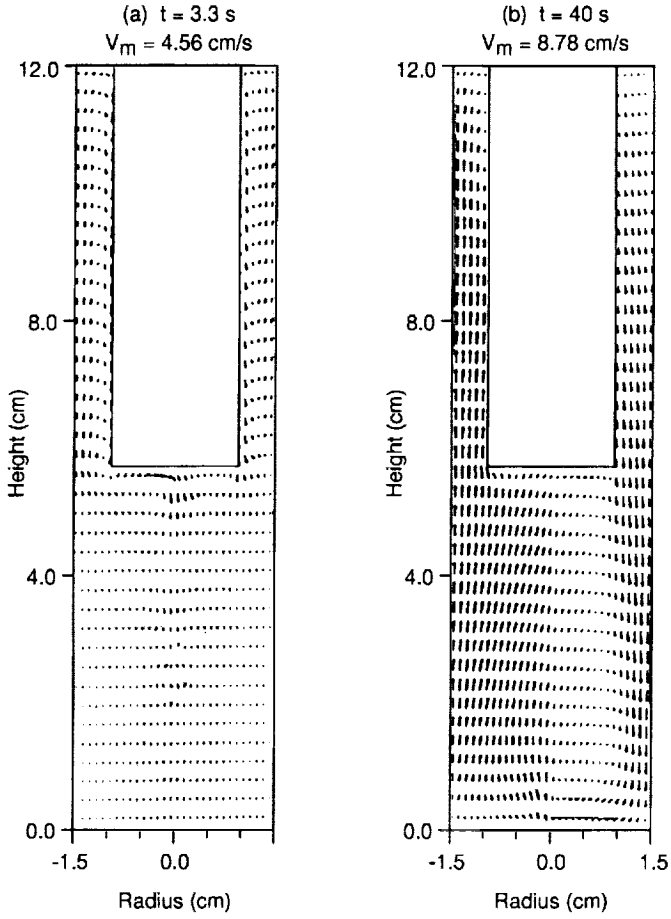

FIGURE 15 Flow in the $\theta = 0°–180°$ plane in a cell in which deposition occurs with the cell tilted 45° to the vertical axis.

$$I = I_0 e^{-\alpha l} \tag{3}$$

where I_0 is incident radiation intensity, I is the reduced radiation intensity after passing through the film, α is a proportionality constant containing the molar absorption coefficient, ε, and concentration of absorber, and l is the film thickness. The molar absorption coefficient represents a molar cross section for absorption. The greater the cross section of the molecule for absorption and absorber concentration, the greater the attenuation of the intensity of the beam. Likewise, film thickness, l also attenuates the beam intensity accordingly. The ratio I/I_0 is a measure of beam transmittance, T. If increased convection yields greater film thickness, we would expect a larger intensity in the absorption bands of films deposited in cells tilted at 45° over those where deposition occurred in cells positioned vertically. We may define the dimensionless product $A = -\alpha l$ as absorbance which incorporates all of the contributors to beam attenuation. Because the nature of the material, DAMNA, and concentration (pure material) are identical in both cases, ab-

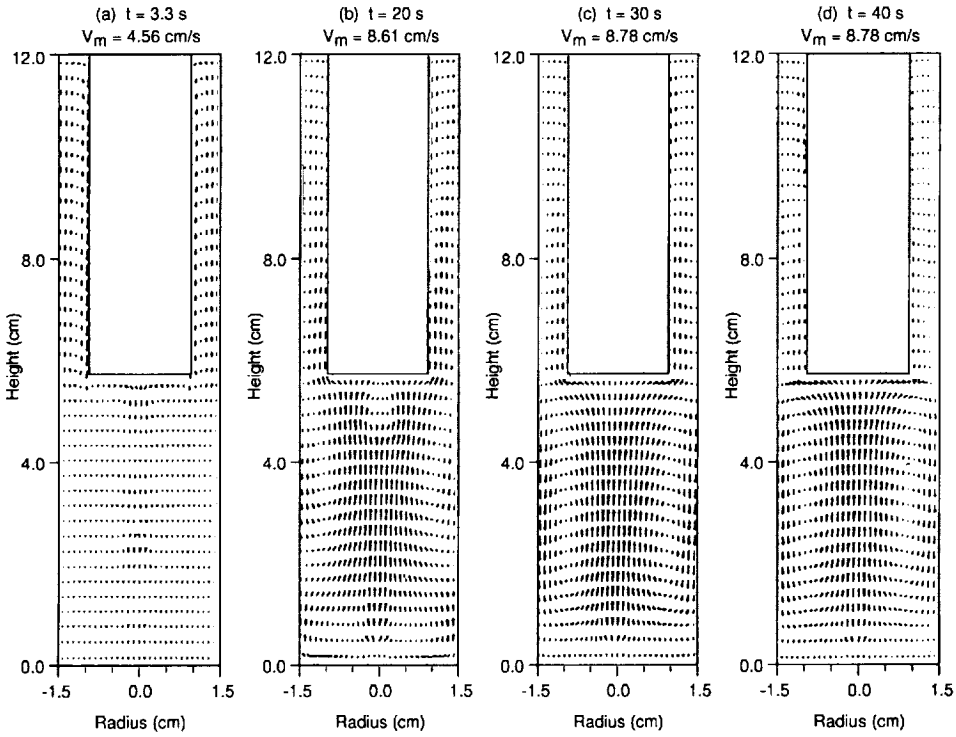

FIGURE 16 Flow in the θ = 90°–270° plane in a cell in which deposition occurs with the cell tilted 45° to the vertical axis.

sorbance is only a function of film thickness. Figure 17 is a wavelength scan in the range 190–820 nm of a vertically deposited film, and Figure 17b is that of an obliquely deposited film. Table 3 contains representative absorbance intensities from scanning an approximately 1-cm-diameter spot in similar vicinities of films formed during vapor deposition in vertically and obliquely oriented cells. Visually, the films from the obliquely oriented cells are a deeper yellow color than those from vertically oriented cells. We qualitatively assume generally thicker films from the relative appearances. The surfaces of these monomer films are translucent and microcrystalline. At the present time, it is also preferable for us to discuss relative film thickness from beam attenuation in qualitative terms (although more quantitative than visual observation) while observing that the spectroscopic irradiation spot sizes are large enough to average over about 50% of the film surfaces. The same relative result occurred, in that beam attenuation was greater at each maximum absorbance wavelength repeatedly. We may consider Table 2 a qualitative representation of a consistent result.

In keeping with the assumptions, the mathematical model correctly predicts qualitative differences in film properties between vertically and obliquely oriented cells; that is, more convection in cells having the tilted orientation is apparently responsible for correspondingly greater film thickness.

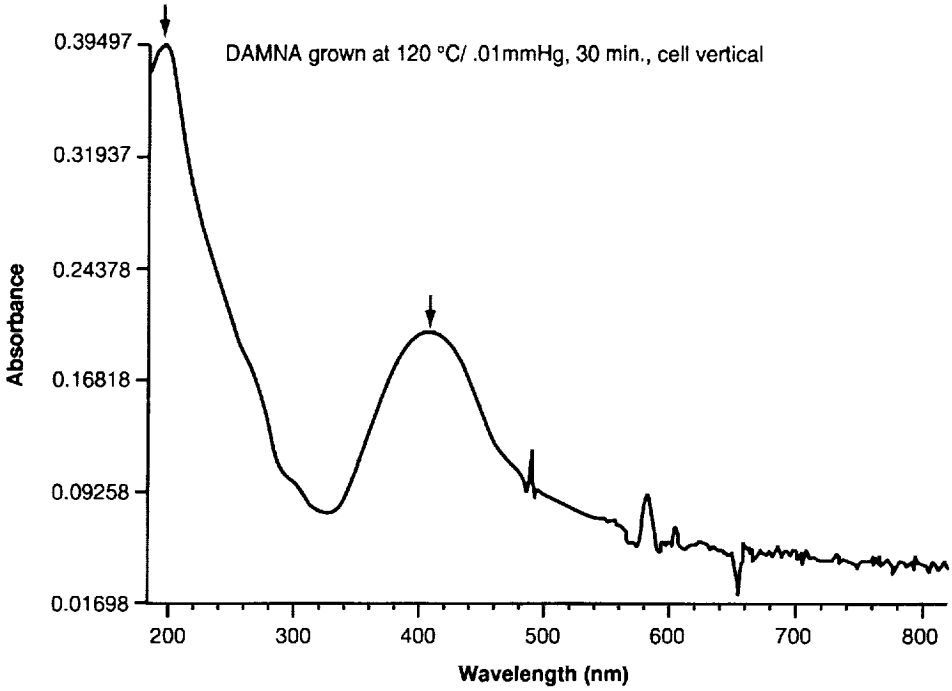

FIGURE 17 Absorbance as function of wavelength for vapor-deposited film after 30 min of deposition for (a) a vertically oriented cell and (b) a tilted cell.

III. GROWTH OF THIN FILMS BY SOLUTION PROCESSES

A. Ultraviolet Solution Polymerization

1. Polydiacetylene Films

Recently, a novel process has been discovered for the formation of thin amorphous polydiacetylene films using photodeposition from monomer solutions onto transparent substrates [45,46,90,101]. Specifically, polymeric films were directly synthesized from a diacetylene monomer, DAMNA (Fig. 12), derived from 2-methyl-4-nitroaniline (MNA) that only sluggishly polymerizes when the crystalline monomer is irradiated [102]. This compound was one of several asymmetric diacetylenes that were first studied extensively for their optical and electronic properties by Garito and co-workers in the late 1970s; however, their investigations did not include behavior in solution [103,104]. It was found that thin polymerized DAMNA (PDAMNA) films can be obtained readily from solutions of DAMNA in 1,2-dichloroethane by irradiation with long-wavelength UV light through a quartz or glass window, which serves as the substrate. This simple straightforward process yields transparent films with thickness on the order of 1 μm.

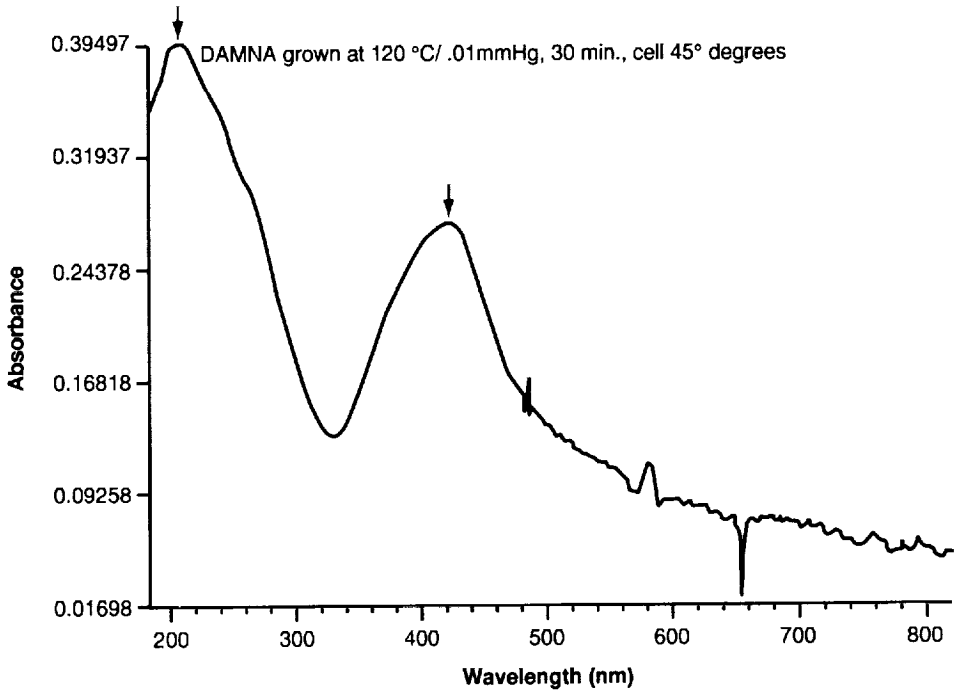

Annotated Wavelength:
1: Wavelength = 422 Result = 0.385361
(b) 2: Wavelength = 214 Result = 0.545670

FIGURE 17 Continued

Despite the considerable volume of literature available on diacetylenes and polydiacetylenes, this solution-state photodeposition reaction has never been reported. Thus, many of the parameters controlling the efficacy of the process are not yet known. The basic idea is quite straightforward; the diacetylene monomer solution is irradiated through a UV transparent substrate and a thin polydiacetylene film results. To date, several diacetylene monomers have been tested and found to be capable of photodeposition of polymeric films from solution.

TABLE 3 Representative Absorbance Intensities from Scanning an Approximately 1-cm-diameter Spot in Similar Vicinities of DAMNA Films Formed During Vapor Deposition

λ (nm)	A_{max} (cell vertical film)	A_{max} (cell tilted film)
422	0.200	0.385
214	0.395	0.546

Special chambers were constructed for carrying out the reaction and obtaining thin films on small round substrate disks (Fig. 18). To obtain a PDAMNA thin film, a solution of DAMNA in 1,2-dichloroethane (approximately 2.5 mg/ml = 0.01 mol/l) is placed inside the chamber, and the chamber is then irradiated through the substrate with long-wavelength UV light (365 nm). The thickness of the resulting PDAMNA film depends on the duration of exposure and the intensity of the UV source. After the photodeposition is complete, the monomer solution, which now also contains suspended particles of precipitated polymer, is removed from the growth chamber. The substrate, now coated on one side with the PDAMNA film, is then removed, washed with 1,2-dichloroethane, and dried.

Thin PDAMNA films obtained in this manner are transparent, glassy yellow–orange in appearance, suggesting an amorphous nature. Both refractive index measurements and electron beam diffraction studies indeed indicate that the films are amorphous. The films are insoluble in organic solvents, although solvents such as acetone can cause them to peel off of the substrate. Even concentrated sulfuric acid does not dissolve the films; they turn brown, shrivel, and peel off of the substrate, but do not dissolve, even after several weeks. In contrast, the PDAMNA powder precipitated from the bulk solution is soluble in solvents such as acetone and dimethylsulfoxide (DMSO).

The exact role that the substrate plays in photodeposition of polydiacetylene films from solution is not yet fully understood. Apparently, any substrate which is sufficiently transparent to UV light can be used; thus far, we have grown PDAMNA films onto glass, quartz, mica, indium–tin-oxide-coated glass, polyethylene teraphthalate, KBr, and NaCl. In order to gain some insight into the process that occurs at the surface of the substrate during photodeposition, masking experiments were conducted in which a portion of the substrate is blocked from exposure to the UV light during film deposition. The mask is placed on the *exterior* surface of the substrate (opposite the side on which the film is grown) and thus, is not in contact with the solution; it serves merely to protect part of the substrate from the light. Interestingly, the result is that film deposition occurs only where the substrate is

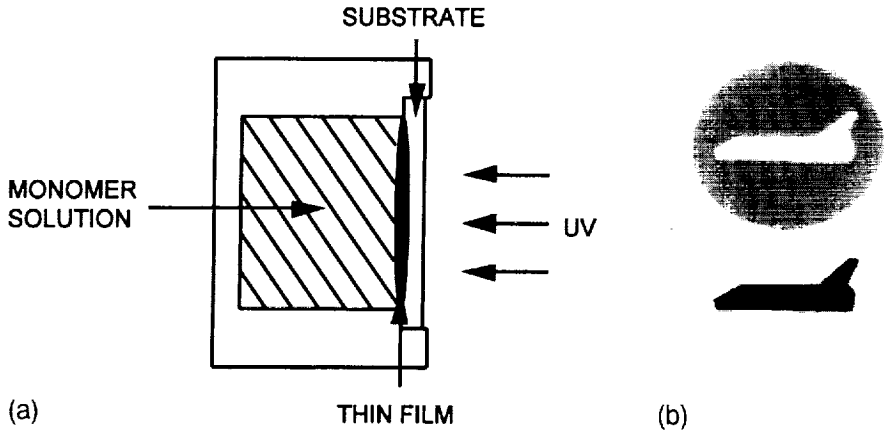

FIGURE 18 (a) Polydiacetylene thin-film growth chamber; (b) masked PDAMNA film on glass.

directly exposed to the light (see Fig. 18b); absolutely no film deposition occurs behind the mask, even though polymerization takes place throughout the bulk solution. This clearly indicates that polymerization is occurring at (or very near) the surface. If this were simply a case of bulk solution polymerization, followed by adsorption of the polymer onto the substrate, the mask, because it is on the outside, should have no effect; film deposition would be expected to occur over the entire substrate.

2. Third-Order NLO Properties of Films

Based on optical microscopy and on refractive index measurements using waveguide mode analysis, PDAMNA thin films obtained via photodeposition from solution have good optical quality, superior to that of films grown using conventional crystal growth techniques. Considering the simplicity of photodeposition, this technique could make the production of polydiacetylene thin films for applications such as nonlinear optical devices technologically feasible. Hence the nonlinear optical properties of the PDAMNA films were investigated—specifically, their third-order NLO susceptibilities.

Degenerate four-wave mixing experiments carried out at 532 nm on PDAMNA films obtained by photodeposition from solution (thickness around 1.0 μm) yield $\chi^{(3)}$ values on the order of 10^{-8}–10^{-7} esu. Qualitative measurements indicate that the response time is on the order of picoseconds, which is consistent with an electronic mechanism for the nonlinearity. It should be pointed out that because 532 nm is in the absorption edge of the polymer, the $\chi^{(3)}$ values obtained are resonance enhanced. Typically, $\chi^{(3)}$ values for polydiacetylenes can vary by several orders of magnitude, depending on the degree of resonance enhancement and other factors [87]. The largest reported nonresonant (purely electronic) $\chi^{(3)}$ value for a polydiacetylene is on the order of 10^{-9}–10^{-10} esu for PTS single crystals [105]. In order to obtain a valid measure of the inherent nonlinearity of the PDAMNA films, experiments need to be conducted at longer wavelengths, where the polymer does not absorb (in the case of PDAMNA, above 700 nm). Preliminary measurements with the PDAMNA films using a Ti–Sapphire laser at 810 nm give $\chi^{(3)}$ values on the order of 10^{-11} esu, with response times on the order of femtoseconds [106]. There are no indications of either one- or two-photon absorption at this wavelength. To ascertain the true potential for device applications (the figures of merit), thorough measurements of light scattering, linear absorption, two- and three-photon absorption, damage thresholds, and so forth must be performed [103]. Such experiments are underway and will be the subject of future publications.

Thus far, these films have not been studied for second-order NLO properties because they are amorphous, although studies (atomic force microscopy, scanning electron microscopy, and UV–visible spectroscopy) do indicate that there is partial chain alignment in the direction normal to the substrate. At present, the degree of orientation is too low to exploit any potential second-order nonlinearity. However, it may be possible to improve the orientation in the films by means such as electric field poling, surface modification of the substrate, or even modifying the polymer structure (e.g., attaching a liquid-crystal moeity). Ordered polydiacetylene films would not only be capable of second-order nonlinearity but should also exhibit increased third-order nonlinearity. Additionally, electronic applications such as one-dimensional conductors require films with aligned polymer chains.

3. Fluid Dynamic Analysis

It is well known that gravitational effects, such as buoyancy-driven convection, can affect heat and mass transport processes in solution [108]. Photodeposition of polydiacetylene films from solution is no exception. We shall first discuss how buoyancy-driven convection can arise during photodeposition of PDAMNA films from solution, and then describe how this convection can affect the morphology, microstructure, and properties of the films obtained. Both the monomer solution and the film generate heat due to absorption of UV radiation. The radiative heating, along with the thermal boundary conditions of the walls of the thin-film growth chamber, will give rise to a complex temperature pattern in the solution. Due to the lack of thermodynamic equilibrium, the solution will possess temperature and concentration gradients, and, therefore, density gradients. These gradients, under the influence of gravity, can induce convective fluid flows in the solution (buoyancy-driven convection).

The onset of thermal convection is determined by a stability parameter known as the Rayleigh number, Ra, defined as [108]

$$\mathrm{Ra} = \frac{\alpha\, g\, d^3\, \Delta T}{\nu\, \kappa} \qquad (4)$$

where α is the coefficient of thermal expansion of the solution, g is the acceleration due to gravity, ΔT is the temperature difference across distance d in the solution, ν is the kinematic viscosity, and κ is the thermal diffusivity. For photodeposition of PDAMNA films, the value of ΔT (over a distance of less than 1 mm) can vary from a only a few tenths of a degree to several degrees, depending on the intensity of the UV radiation. In order to grow thicker films (>1 μm), higher-intensity radiation is necessary, making large temperature gradients unavoidable. The intensity and flow pattern of convection can be predicted when the Rayleigh number is known. For instance, for an infinite fluid layer in the horizontal direction with a temperature gradient in the vertical direction (colinear with gravity), convective motion will occur in the form of rolls with axes aligned horizontal when Ra > 1708 (the critical Rayleigh number), whereas no convection will occur if Ra < 1708 [109]. The exact value can only be determined by numerical solution of the fluid flow in the chamber. In the case of horizontal temperature gradients (orthogonal to gravity), all values of the Rayleigh number lead to convection, and the magnitude of the velocity of the fluid flow is proportional to the square root of the Rayleigh number.

Density gradients can also arise in the solution due to variations in the concentrations of the chemical species present in the solution. Variations in the monomer concentration are caused by depletion of monomer from the solution at the surface of the growing film and in the bulk. Also, generation of dimers, trimers, and other soluble by-products in the bulk solution may result in additional concentration density gradients. Such solutal gradients, along with the temperature gradients, can give rise to double-diffusive convection. This complicated convective motion is usually analyzed with the aid of the solutal Rayleigh number, in addition to the thermal Rayleigh number [108]. The solutal Rayleigh number, Ra_s, is defined as

$$\mathrm{Ra}_s = \frac{\beta\, g\, d^3 \Delta C}{\nu\, D} \tag{5}$$

where β is the coefficient of concentration expansion, ΔC is the concentration difference across distance d in the solution, and D is the diffusion coefficient. Double-diffusive convection flows can be far more complex than simple thermal convection flows.

Hence, we see that convection can arise by several means during polydiacetylene film photodeposition from solution. The extent of convection and its intensity and structure can only be understood through accurate numerical modeling of the fluid motion and thermodynamic state of the system.

4. Transport of Particles from Bulk Solution

One significant effect of convection can be seen when PDAMNA films grown in 1-**g** are viewed under an optical microscope: They exhibit small particles of solid polymer embedded throughout. These form when polymer chains in the bulk solution collide due to convection and coalesce into small solid particles, on the order of a few hundredths of a micrometer in size. Because these particles are so small, almost colloidal in nature, they do not sediment out readily and, thus, remain suspended in the bulk solution. Convection then transports these particles to the surface of the growing film, where they become embedded. These particles are defects that can scatter light and, thus, lower the optical quality of the films.

To study the effects of convection on the occurrence of these particles in the films, the growth chamber was placed in different orientations with respect to gravity in order to vary the fluid flow pattern [110]. PDAMNA films were grown with the chamber vertical (irradiating from the top) and with the chamber horizontal (irradiating from the side). In the case when the chamber is vertical and the solution is irradiated from the top, the axial temperature gradient is vertical with respect to gravity, and the bulk solution is stably stratified because warmer, less dense solution is above cooler, more dense solution. Thus, in this orientation, convection should be minimized. In the case when the chamber is horizontal and the solution is irradiated from the side, the axial temperature gradient is horizontal with respect to gravity, which makes the density gradients less stable. Hence, convection should be much more pronounced in this orientation. Numerical simulations of the fluid flow are consistent with these expectations [110].

This is reflected in the distribution of solid particles observed in the PDAMNA films grown in the two different orientations. Films grown with the chamber horizontal clearly contain a greater concentration of particles than films grown with the chamber vertical (Fig. 19). This is consistent with expectations based on the relative amounts of convection in the two orientations; films grown under increased convection contain more particles than those grown under less convection. Also, waveguiding experiments with these films demonstrate that the films containing more particles exhibit greater light scattering than those containing fewer particles.

Note that even the film grown in the vertical orientation, where convection is minimized, still contains particles. Thus, although convection is lessened in this case, it is not eliminated. There are two reasons for this. First, there are still radial thermal density gradients in the horizontal direction, even when the chamber is

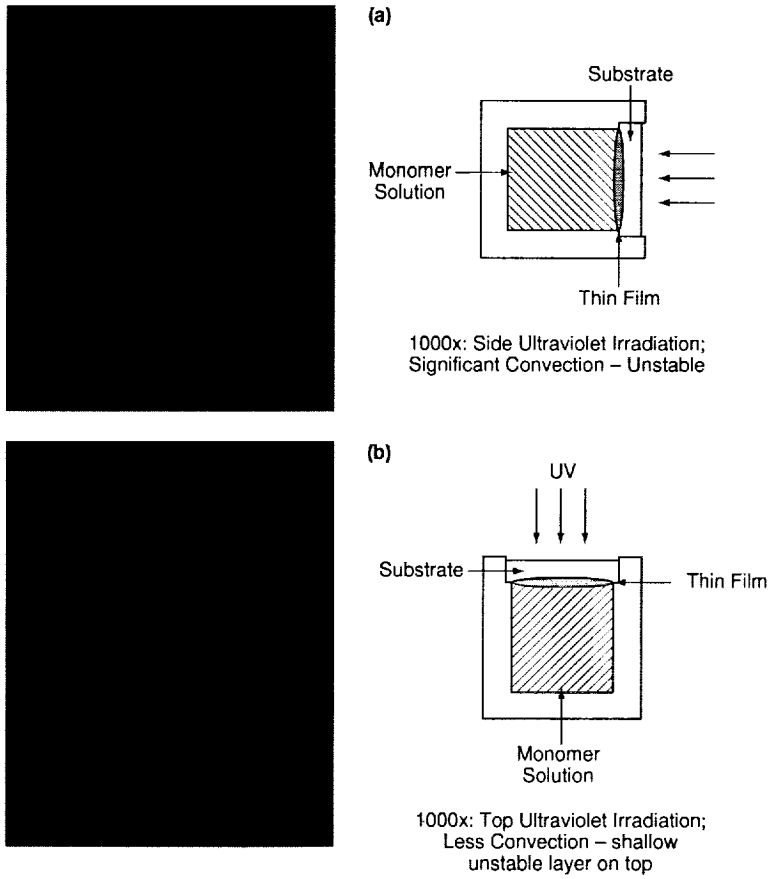

FIGURE 19 PDAMNA films grown in two different orientations: (a) films grown with the chamber horizontal; (b) films grown with the chamber vertical.

vertical because the solution near the side walls is cooler than that near the center; these can give rise to convection. Also, because the substrate is transparent to UV light, it is not heated directly by the radiation; the only means by which it receives heat is via conduction. Thus, initially, there will be some heat flow from the warm solution to the cooler substrate, producing a very shallow unstable thermal density gradient in the immediate vicinity of the substrate–solution interface, which sits above the stably stratified bulk solution. Any convection initiated in this unstable layer may penetrate deeper into the stable layer below, giving rise to the phenomenon of penetrative convection [111]. The bottom line is that even under optimum conditions in 1 **g**, convection is still present during polydiacetylene thin film photodeposition from solution, causing particles in the films.

Not only can convection affect the transport of particles which are polymerized from the bulk solution, it can also transport colloidal particles which are purposely introduced into the system to alter the optical properties. The study of the effect

of composite geometry on the nonlinear optical properties of materials is an active area of research. One of the most commonly studied systems, discussed earlier, involves small metal inclusion particles surrounded by a continuous host medium. The linear optical properties of these composites are described by the theory of Maxwell Garnett [112]. In recent years, the model has been extended to include nonlinear materials [113,114]. Unfortunately, assimilation of metal particles into highly nonlinear solid-state materials is difficult using traditional chemical techniques because most highly nonlinear polymeric host candidates require organic solvents which are incompatible with the colloid. Ion implantation is a realistic alternative but is not readily available in most laboratories. Moreover, the distribution of metal in the axial direction follows a Gaussian profile. Recently, however, Brust et al. [115], functionalized gold particles with thiol groups which serve to protect the particles from solvent degradation and attack. Interestingly, the colloidal metal can actually be dried and stored without agglomeration. The thiol groups in this case have little effect on the optical properties of the colloid. These thiol-capped metal particles can then be resuspended in many organic solvents and incorporated into the PDAMNA films through photopolymerization. Hence, this recipe offers a simple way to introduce small metal particles into highly nonlinear polymers. The resulting films, however, suffer from gradients in the metal concentration which are clearly visible under reflected room light. Moreover, the films have a much higher concentration of metal than would be expected from a diffusional process. Hence, these gradients most likely arise from the process of convection. Convection often tends to destroy the homogeneity of particle-doped systems, whether it be colloidal metal films or doped porous glass. In this case, the metal particle dopants serve not only to modify the nonlinear optical properties of the system but also to elucidate the role of convection in the formation of polymeric thin films.

5. Effects of Convection of Kinetics, Morphology, and Microstructure

We have discussed how convection can transport particles of solid polymer precipitated from the bulk solution into the films. However, convection can also affect film deposition at the molecular level. To gain some insight into these effects, it is necessary to understand the kinetics of film deposition.

The rate of polydiacetylene film photodeposition from solution can be given by the expression [116]

$$\frac{dl}{dt} = kI^m C^n \tag{6}$$

where l is film thickness, t is time, I is the intensity of the UV radiation, C is monomer concentration, m and n are the orders of the reaction in radiation intensity and monomer concentration, respectively, and k is the rate constant. Initial results indicate that for photodeposition (using 365-nm-wavelength light) of PDAMNA films from 1,2-dichloroethane at ambient temperature (25°C), $m = 1.0$, $n = 0.5$, and $k = 3.2 \times 10^{-7}$ (MKS units) [117].

Additionally, it can be shown from the principles of chemical kinetics (Arrhenius equation) [116] that the rate constant (k) is given by

$$k = Ae^{-E/k_bT} \tag{7}$$

where E is the activation energy of the reaction, k_b is Boltzman's constant, T is temperature, and A is a preexponential factor related to the frequency of collisions of molecules with the surface of the growing film.

The equations above clearly show how the rate of polydiacetylene film photodeposition from solution depends on variables such as temperature and monomer concentration. The effects of convection can also be gleaned from these equations. We know that convection affects heat and mass transport to and from the surface of the growing film, which is reflected in the temperature and concentration profiles along the surface. Variations in these parameters along the surface of the film, in accordance with the above equations, will cause variations in the rate of film deposition, leading to uneven film growth. This will be especially pronounced if the fluid flow along the surface varies drastically or is turbulent. Thus, we see how convection can directly affect the kinetics of polydiacetylene film photodeposition from solution, and thereby affect the morphology (thickness and surface roughness) of the films.

Finally, convection may also play a role in affecting the microstructure of the films, specifically the molecular orientation of the polydiacetylene chains. Preliminary studies conducted using atomic force microscopy and x-ray photoelectron spectroscopy indicate that films photodeposited onto quartz (in 1 **g**) for a very short duration of time (a few minutes) exhibit good polymer-chain alignment in the direction normal to the substrate, whereas films grown for longer duration show significantly poorer chain alignment. Thus, in the early stages of deposition, there appears to be some tendency for orientation, which lessens as the reaction proceeds and the polymer chains grow. This could be due to the fact that as the film grows, any influence that the substrate may have on molecular orientation at the film surface decreases. However, in this case, the substrate is amorphous quartz; hence, ordering of the polymer chains by the substrate (i.e., epitaxy) is not expected. Therefore, another possibility for the decrease in order is convection. The turbulent and chaotic molecular motions that occur during convection may cause the chains to become entangled and matted around each other as they grow longer. Also, variations in temperature and monomer concentration along the film surface, influenced by convection, can effect molecular orientation, and possibly even polymer-chain packing densities. Discerning the role that convection plays in affecting molecular orientation is an essential part of any fundamental study.

6. Growth of Films in Microgravity

An experiment was recently conducted aboard the Space Shuttle Endeavor (CONCAP-IV) in which photodeposition of PDAMNA films from solution was carried out in microgravity [114]. In this environment, buoyancy-driven convection can essentially be eliminated. Because of unplanned orbiter maneuvers during the mission, leading to extraneous accelerations and limitations of the flight hardware, results varied somewhat among samples. However, the best space grown film clearly exhibits fewer particles than the best ground-based films (Fig. 20). These few particles may have resulted from slight mixing in the solution caused by the orbiter motions, or, possibly, they may have nucleated on the surface of the film itself. Nonetheless, the initial results are very encouraging; it appears that the lack of convection can, indeed, lead to PDAMNA films with significantly fewer defects,

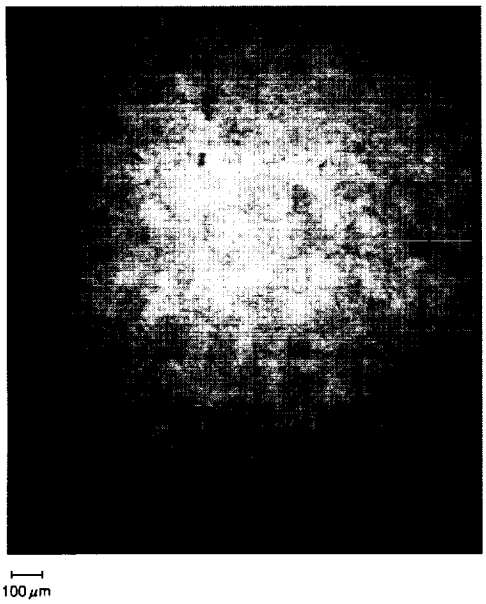

FIGURE 20 PDAMNA films grown in space. The best space grown films clearly exhibit fewer particles than the best ground-based films.

and thus greater optical quality. Further characterizations of the space grown films are currently underway.

This study clearly shows that photodeposition of polydiacetylene thin films in unit gravity occurs in highly convective environments and that this convection can influence the morphology and quality of the films. Indeed, even when irradiation occurs from the top of the cell, the most stable stratified cell orientation, defects remain in the films due to the persistence of buoyancy-driven convection. To achieve homogeneity, minimal scattering centers, and possible molecular-order photodeposition of polymer films by UV light exposure must proceed in a microgravity environment. Fluid mechanics simulations are useful for establishing gravitational sensitivity to this recently discovered process [45] for preparing thin films having quite promising nonlinear optical characteristics.

B. Polymer Thin Films by Electrochemical Polymerization

Electrochemical polymerization is a method that should be thoroughly investigated for use in fabricating thin-film waveguides. The procedure is relatively straightforward and films can be fabricated using many commercially available materials. Another desirable feature is that NLO films might be prepared on the surface of various substrates during polymerization for the fabrication of devices. In addition, this method has been used to synthesize several polymers that include polythiophenes, polypyrrole, polazulene, and polypyrrole.

Polythiphenes (pT) are promising materials for NLO applications because of their large third-order optical nonlinearities, environmental stability, and structural

versatility. Their potential suitability for devices was demonstrated by Dorsinville et al. [118], who measured the NLO properties of thin films of pT, polythieno(3,2-b), thiophene (pTT), polydithieno(3,2-b,2′,3′-d)thiophene (pDTT). The $\chi^{(3)}$ values at 532 nm for pT, pTT, and pDTT were 6.6×10^{-9} esu, 5.9×10^{-9} esu, and 11.3×10^{-9} esu, respectively. Electropolymerization of the monomers was performed in a two-compartment cell with indium–tin oxide electrodes. Typical thickness of films were 0.5–2 μm. In addition, Logsdon et al. [119] obtained a $\chi^{(3)}$ value of 10^{-9} esu for LB films of poly(3-dodecylthiophene). The polymer was first prepared by electrochemical polymerization. This was then used to prepare LB films. The electrochemical process was carried out at 5°C using nitrobenzene as the solvent, tetra-*n*-butylammonium hexaflurophosphate as the electrolyte, indium–tin oxide as the cathode, and a platinum coil as the cathode.

The prospect for using microgravity processing to produce better polymer films by electrochemical reactions or learn principles that might be used to improve processing on Earth should be explored, as there is evidence that electrodeposition of metals in low gravity results in deposits that have significant differences relative to those prepared on Earth. Ehrhard [120,121] found that nickel deposited at high rates in microgravity during a suborbital rocket flight produced an amorphous or nanocrystalline film with grains so small that x-ray diffraction peaks associated with the crystalline structures were not seen. Further studies involving the electrodeposition of metals in microgravity have been performed by Riley and co-workers [122–124].

IV. PROTOTYPE DEVICES BASED ON SECOND- AND THIRD-ORDER NLO ORGANICS AND POLYMERS

A. Electrooptic Polymer Advances

It is an accepted conclusion that the development of all-optical devices will be gradual and will include hybrid devices in which electrons interface with photons. The advent of electrooptics occurred several years ago when researchers realized that photons could respond to electrons through certain media such as lithium niobate ($LiNbO_3$). This route toward the development of all-optical devices demands immediate and intensive searches for the ideal hybrid, which requires large second-order characteristics in the materials of interest and appropriate processing techniques. It is this technology requirement that enhances the criticality of asymmetry in crystal packing and heightens the potential value of microgravity processing. The goal is to exploit maximum and optimal directionality of hyperpolarizabilities in inorganic or organic crystals interacting with electric fields, and their capacity to modulate light. Alignment of polymers and macromolecules to take advantage of predicted second-order superiority in many of these molecules could provide the desired effects.

There have been several significant advances in the development of electrooptic devices based on polymers. One of the problems associated with organic systems is the inherent "brittle" nature of pure materials as a result of weak van der Waals intermolecular interactions in contrast to strong ionic and covalent bonds characteristic of inorganics. Dalton et al. [125] have addressed this problem by preparing a variety of highly cross-linked polymers based on spin-casting and poling a poly-

methacrylate with "dangling chromophores." The resultant cross-linked polymer films are "hard" and exhibit very high electrooptic coefficients. These materials retain their optical nonlinearity for several thousand hours at relatively high temperatures (90–150°C). Optoelectronic modulators developed by this group based on these and other materials and processes are available as prototypes and are capable of efficiently converting electronic signals into optical signals. These researchers and some others in the field believe that polymer-based modulators will outperform conventional inorganic devices and should be significantly less expensive to prepare. Marder and co-workers [126] have played a key role in these developments, including the development of a heterocyclic molecule with a strong electron donor and strong acceptors. This molecule is highly soluble in a polycarbonate matrix, which, after poling, yields a material with very high second-order coefficients and good mechanical strength. Although this material does not have good thermal stability, the contribution is a significant one toward the search for the ideal electrooptic material based on organic and polymeric materials.

B. All-Optical Switching

A Mach–Zehnder (MZ) interferometer (Fig. 21a) is an example of an on–off switch. Switching occurs when the phase of one arm is shifted by π relative to the phase of the other arm. For all-optical switching, the phase shift may be achieved by introducing a NLO material into one of the arms of the interferometer or by using a nonlinear material for the entire interferometer and making one arm longer than the other—an asymmetric MZ. For fused silica fibers, long lengths of fiber are required to reduce the switching energy due to the weak nonlinearity, and this makes it difficult to maintain the stability of the interferometer. Thus, for fibers, a very ubiquitous approach is to use a nonlinear optical loop mirror (Fig. 21b). The loop mirror is very stable, as it is a common path interferometer. The required phase shift is achieved through cross-phase modulation (XPM) of the signal by an orthogonal polarized control pulse. Because the control pulse propagates in one direction, the index change occurs only for the copropagating signal pulse. The bottom coupler extracts the control pulse from the loop.

Although NLO loop mirrors provide a variety of controls and options for the user, more compact devices are required for integrated optics applications and these require materials with higher nonlinearity to keep the switching energy low enough to be practically useful. The nonlinear directional coupler described earlier (Fig. 21c) or the Mach–Zehnder interferometer are better suited for these applications. Efficient femtosecond all-optical switching has been demonstrated in GaAlAs passive semiconductor systems at energies below half the band gap in a number of different devices [127–130]. Although TPA is no longer a problem for energies below half the band gap, three-photon absorption can still impede (degrade) device performance [131]. To avoid three-photon absorption, Stegeman et al. employed a longer interaction length in an NLDC to reduce the switching power, thus avoiding higher-order nonlinear absorption [132]. A switching energy of 65 pJ was achieved. GVD had little effect for 6.6-ps pulses but severely affected device operation for 430-fs pulses. An important trait of these semiconductor systems is that by varying the alloy composition, the half-band-gap energy can be tuned anywhere within the telecommunications window of 1.3–1.6 μm. An alternative approach to working

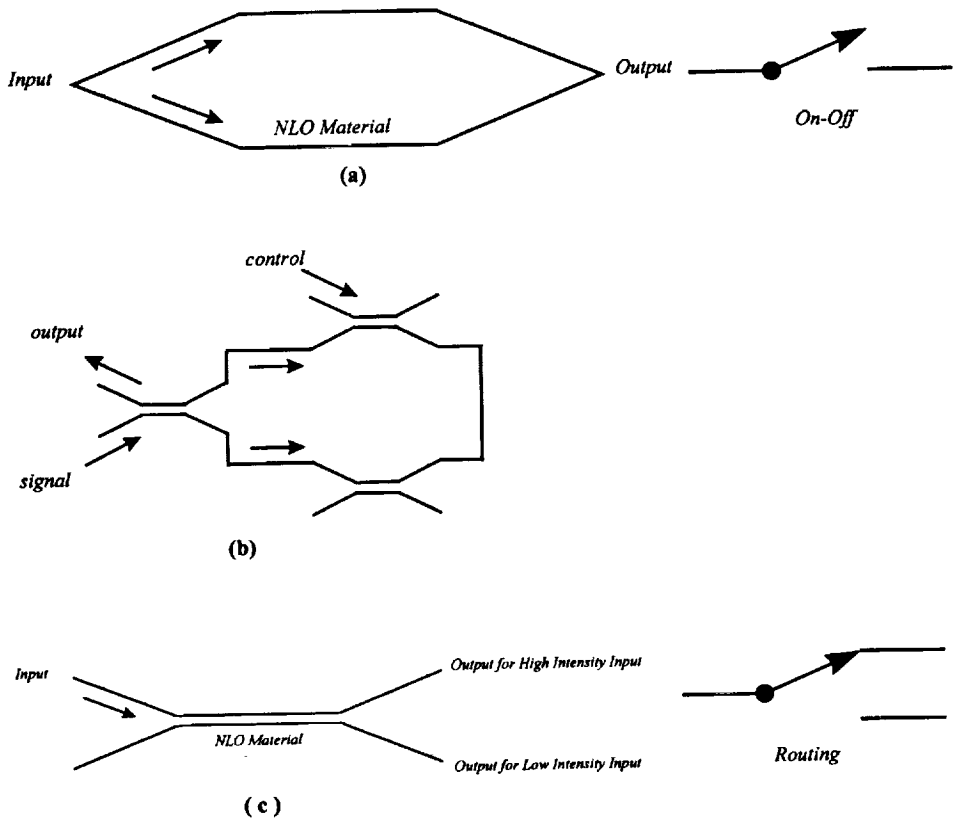

FIGURE 21 (a) Mach–Zehnder interferometer; (b) nonlinear optical loop mirror; (c) nonlinear directional coupler and their electronic analogs.

below the half-band-gap presented is to utilize the large, fast nonlinearity at the transparency point of an active semiconductor. Lee et al. have reported subpicosecond 10-pJ switching at 880 nm in a current injected GaAs/AlGaAs multiple-quantum-well NLDC [133].

Organic materials such as conjugated polymers, although less developed than semiconductor systems, are highly promising because they generally have larger nonlinearities, are more facile for molecular tailoring, and more malleable then their inorganic counterparts. Many conjugated polymers are difficult to pattern into waveguides, however, and it was nearly a decade before switching in an NLDC made from a soluble polydiacetylene commonly known as poly(4-BCMU) (poly-[5,7-dodecadiyne-1,1,12-diolbis(*n*-butoxycarbonylmethylurethane)]) was assessed by Townsend et al. [134]. An interesting fabrication technique was utilized in which the substrate was first patterned with high-index ion-exchanged channels before spin-coating. The underlying channel provides lateral optical confinement, requiring no patterning of the polymer itself. However, because refractive index of the polymer is higher than that of the channels, the polymer contains the majority of the field and, hence, provides the necessary nonlinear optical interactions. Although a

slower thermooptical switching was attained, incomplete ultrafast switching at 1.06 μm was observed due to TPA. Irreversible photo-induced bleaching has also been shown to produce index changes in poly(4-BCMU) that are large enough to fabricate channel waveguides [135]. In addition to expected enhancement of $\chi^{(3)}$ and possible $\chi^{(2)}$ inducement through microgravity processing by certain techniques as discussed, it is viable to encourage self-ordering characteristics of liquid-crystal molecules into the polydiacetylene structure. Such would facilitate the formation of ordered thin films, particularly during microgravity processing by, for example, the photodeposition process. Thakur et al. have demonstrated all-optical phase modulation in a polydiacetylene by using a photolithographic technique to fabricate channel waveguides in single-crystal films of PTS prepared by a shear method [104]. The figures of merit of PTS at the communications wavelengths of 1.3 μm and 1.55 μm have been measured by Kim et al. and indicate its promise for all-optical switching applications [136]. More recently, it has been demonstrated that PDAMNA films photodeposited from solution (described earlier) may be exploited to produce integrated optical structures [45,46].

With only marginal improvements in the GaAs/AlGaAs passive semiconductors expected in the near future, attention has turned to the polymeric systems. Although the technology of fabricating third-order polymeric integrated optics is still maturing, the figures of merit are very promising. We believe that, because of the uniqueness of polymeric materials, simpler and less costly techniques such as those presented here can develop, eventually complementing standard lithographic techniques.

ACKNOWLEDGMENTS

The authors are grateful for support from NASA's Office of Life and Microgravity Science and to Hari Sunkara for helpful suggestions after reviewing the manuscript.

REFERENCES

1. Nayar, B. K., and Winter, C. S., *Opt. Quantum Electron., 22*, 297 (1990).
2. Carter, G. M., Chen, Y. J., and Tripathy, S. K., *Appl. Phys. Lett., 43*, 891 (1988).
3. Kajzar, F., Meissier, J., Zyss, J., and Ledoux, I., *Opt. Commun., 45*, 133 (1983).
4. Kajzar, F., and Messler, J., *Thin Solid Films, 11*, 132 (1988).
5. Debe, M. K., and Kam, K. K., *Thin Solid Films, 816*, 289 (1990).
6. Frazier, D. O., Penn, B. G., Witherow, W. K., and Paley, M. S., *Crystal Growth in Space and Related Diagnostics, 1557*, 86 (1991). San Diego, CA, 22–23 July 1991.
7. Wegner, G. Z., *Naturforschung, 246*, 824 (1969).
8. Thakur, M., and Meyler, S., *Macromolecules, 18*, 2341 (1985).
9. Thakur, M., Carter, G. M., Meyler, S., and Hryniewicz, H., *Polym. Prepr., 27*(1), 49 (1986).
10. Ledoux, I., Josse, D., Vidakovic, P., and Zyss, J., *Opt. Eng., 27*(1), 49 (1986).
11. Islam, M. N., *Phys. Today, 47*(5), 34 (May 1994).
12. Franken, P. A., Hill, A. E., Peters, C. W., and Weinreich, G., *Phys. Rev. Lett., 7*, 118 (1961).
13. Davydov, L. D., Derkacheva, V. V., Dunina, M. E., Zhabotinskii, V. F., Zolin, L. G., Koreneva, and Samokhina, M. A., *Opt. Spectrosc., 30*, 274 (1971).

14. Marcy, Rosker, M. J., Warren, L. F., Cunningham, P. H., Thomas, C. A., Deloach, L. A., Velsko, S. P., Ebbers, C. A., Liao, J. H., and Kanatzidis, M. G., *Opt. Lett. 20*, 252 (1995).
15. Rosenberger, F., Howard, S. B., Sowers, J. W., and Nyce, T. A., *J. Crystal Growth, 129*, 1 (1993).
16. Pusey, M., Witherow, W., and Naumann, R., *J. Crystal Growth, 90*, 105 (1988).
17. Pusey, M., in *Fourth International Conference on Crystallization of Biological Macromolecules*, Freiburg, Germany, Aug. 18–23 1991.
18. Agrawal, G. P., *Nonlinear Fiber Optics*, Academic Press, San Diego, CA 1995.
19. Jensen, S. M., *IEEE J. Quantum Electron., QE-18*, 1580 (1982).
20. Mizrahi, V. K., Delong, K. W., Stegeman, G. I., Saifi, M. A., and Andrejco, M. J., *Opt. Lett., 14*, 1140 (1989).
21. Sheik-Bahae, M., Hagan, D. J., and Van Stryland, E. W., *Phys. Rev. Lett., 65*, 96 (1990).
22. Delong, K. W., and Stegeman, G. I., *Appl. Phys. Lett., 57*, 2063 (1990).
23. Hache, F., Richard, D., Flytzanis, C., and Kriebig, U., *Appl. Phys. A47*, 47 (1988).
24. Lehoczky, S. L., Szofran, F. R., Gillies, D. C., Cobb, S. D., Su, C. H., Sha, Y. G., and Andrews, R. N., *NASA Conf. Publi., 3272* (1994).
25. Smith, D. D., *Ph.D. thesis*, University of Alabama in Huntsville (1996).
26. Turkevich, J., Stevenson, P. C., and Hillier, H., The Size and Shape Factor in Colloidal Systems, *Disc. Faraday Soc., 11*, 55 (1951).
27. Fröhlich, H., *Theory of Dielectrics*, Oxford University Press, London 1958.
28. Swatton, S. N. R., Welford, K. R., Till, S. J., and Sambles, J. R., *Appl. Phys. Lett., 66*, 1868 (1995).
29. Stegeman, G. I., and Miller, A., in *Photonics and Switching*, (J. E. Midwinter, ed.), Academic Press, London, 1994, p. 81.
30. Delong, K. W., Rochford, K. B., and Stegeman, G. I., *Appl. Phys. Lett., 55*, 1823 (1989).
31. Yang, C. C., Villeneuve, A., Stegeman, G. I., and Aitchison, J. S., *Opt. Lett., 17*, 710 (1992).
32. Asobe, M., Naganuma, K., Kaino, T., Kanomori, T., Tomaru, S., and Kurihara, T., *Appl. Phys. Lett., 64*(22), 2922 (1994).
33. Paley, M. S., Frazier, D. O., McManus, S. P., Zutaut, S. E., and Sangahadasa, M., *Chem. Mater. 5*, 1641 (1993).
34. Debe, M. K., *Prog. Surf. Sci, 24*(1–4), 1 (1987).
35. Liu, C. J., Debe, M. K., Leung, P. C., and Francis, C. V., *Appl. Phys. Commun. 11*(2&3), 151 (1992).
36. Kam, K. K., Debe, M. K., Poirer, R. J. and Drube, A. R., *J. Vac. Sci. Technol., A5*(4), 1914 (1987).
37. Debe, M. K., Kam, K. K., Liu, C. J., and Poirier, R. J., *J. Vac. Sci. Technol., A6*, 1907 (1988).
38. Debe, M. K., *J. Appl. Phys., 55*, 3354 (1984); Debe, M. K., and Tommet, T. N., *J. Appl. Phys., 62*, 1546 (1987).
39. Debe, M. K., Poirier, R. J., and Kam, K. K., *Thin Solid Films, 197*, 335 (1991).
40. Debe, M. K., and Field, D. R., *J. Vac. Sci. Tehcnol., A9*, 1265 (1991).
41. Debe, M. K., *J. Vac. Sci. Technol., A10*(4), 2816 (1992).
42. Debe, M. K., *J. Vac. Sci. Technol., 21*, 74 (1992).
43. Debe, M. K., Poirier, R. J., Erickson, D. D., Tommet, T. N., Field, D. R., and White, K. M., *Thin Solid Films, 186*, 257 (1990).
44. Debe, M. K., and Poirier, R. J., *Thin Solid Films, 186*, 327 (1990).
45. Paley, M. S., Frazier, D. O., McManus, S. P., and Donovan, D. N., U.S. Patent 5,451,433 (September 19, 1995).

46. Paley, M. S., Frazier, D. O., Abdeldeyem, H. A., Armstrong, S., McManus, S. P., *J. Am. Chem. Soc.*, *117*(17), 4775 (1995).
47. Pearson, E., Witherow, W. K., and Penn, B. G., personal communication.
48. Hotta, S., Hosaka, T., Soga, M., and Shimotsuma, W., *Synth. Met.*, *9*, 381 (1984).
49. Tanaka, S. M., Sato, A., and Kaeriyama, K., *Makromol. Chem. 185*, 1295 (1984).
50. Waltman, R. J., and Bargon, J., *Can. J. Chem.*, *64*, (1986).
51. Yang, L., Dorsinville, R., Wang, Q. Z., Zou, W. K., Ho, P. O., Yang, N. L., Alfano, R. R., Zamboni, Z., Danieli, R., Ruani, G., and Taliani, C., *J. Opt. Soc. Am.*, *6*(4), 753 (1989).
52. Dorsinville, R., Yang, L., Alfano, R. R., Zanboni, Z., Daniel, R., and Taliani, C., *Opt. Lett.*, *14*(23), 1321 (1989).
53. Abi-Akar, H. M., Ph.D. thesis, University of Alabama in Huntsville (1992).
54. Abi-Akar, H., Riley, C., Coble, H. D., and Maybee, G., (private communication).
55. Ho, Z. Z., Ju, C. Y., and Hetherington, W. M., III., *J. Appl. Phys.*, *62*, 716 (1987).
56. Shirk, J. S., Lindle, J. R., Bartoli, F. J., Hoffman, C. A., Kafafi, Z. H., and Snow, A. W., *Appl. Phys. Lett.*, *55*, 1287 (1989).
57. Wu, J. W., Heflin, J. R., Norwood, R. A., Wong, K. Y., Zamani-Khamiri, O., Garito, A. F., Kalyanaraman, R., and Sounik, J., *J. Opt. Soc. Am. B*, *6*(4), 707 (1989).
58. Matsuda, M., Okada, S., Masaki, A., Nakanishi, H., Suda, Y., Shigehara, K., and Yamada Y., Proc. SPIE, *1337*, 1995 (1990).
59. Hosoda, M., Wada, T., Yamada, A., Garito, A. F., and Sasabe, H., *Jpn. J. Appl. Phys.*, *30*, L1486 (1991).
60. Hoshi, H., Nakamura, N., and Maruyama, Y., *J. Appl. Phys.*, *70*, 7244 (1991).
61. Suda, Y., Shiegehara, K., Yamada, A., Matsuda, H., Okada, S., Masaki, A., and Nakanishi, H., Proc. SPIE, *1560*, 75 (1991).
62. Casstevens, M. K., Samoc, M., Pfleger, J., and Prasad, P. N., *J. Chem Phys.*, *92*, 2019 (1990).
63. Prasad, P. N., and Williams, D. J., *Introduction to Nonlinear Optical Effects in Molecules and Polymers*, Wiley–Interscience, New York, 1991, p. 205.
64. Roger, J. R., Powell, R. C., Chang, Y. H., Ford, W. T., and Zhu, W., *Opt. Mater.*, *5*, 43 (1996).
65. Ho, Z. Z., and Peyghambarian, N., *Chem. Phys. Lett.*, *148*, 107 (1988).
66. Williams, V. S., Mazumdar, S., Armstrong, N. R., Ho, Z. Z., and Peyghambarian, N., *J. Phys. Chem.*, *96*, 4500 (1992).
67. Wada, T., Matsuoka, Y., Shigehara, K., Yamada, A., Garito, A. F., and Sasabe, H., Mater. Res. Socl Symp. Proc., *12*, 75 (1989).
68. Shirk, J. S., Lindle, J. R., Bartoli, F. J., Hafafi, Z. H., Snow, A. W., and Boyle, M. E., *Int. J. Nonlinear Opt. Phys.*, *1*, 699 (1992).
69. Sastre, A., Torres, T., Diaz-Garcia, M. A., Aguillo-Lopez, F., Dhenqant, C., Brasselet, S., Ledoux, I., and Zyss, J., *J. Am. Chem. Soc.*, *118*, 2746 (1996).
70. Suslick, K. S., Chcn, C. T., Meredith, G. R., and Cheng, L. P., *J. Am. Chem. Soc.*, *114*, 6928 (1992).
71. Li, D., Swanson, B. I., Robinson, J. M., and Hoffbarrer, M. A., *J. Am. Chem. Soc.*, *115*, 6975 (1993).
72. Wada, T., Yamanda, S., Matsuoka, Y., Grossmn, C. H., Shigehara, K., Sasbe, H., A., Yamada, and Garito, A. F., in *Nonlinear Optics of Organics and Semiconductors* (T. Kobayashi, ed.), Springer-Verlag, Berlin, 1989, p. 292.
73. Hosada, M., Wada, T., Yamada, A., Garito, A., and Sasabe, H., *Jpn J. Appl. Phys.*, *30*(8B), L1486 (1991).
74. Chollet, P. A., Kajzar, F., and LeMoigne, J., Proc. SPIE, *1273*, 87 (1990).
75. Kumagai, K., Mitzutani, G., Tsukioka, H., Yamauchi, T., and Ushioda, S., *Phys. Rev. B*, *48*(19), 14488 (1993).

76. Yamada, T., Hoshi, H., Ishikawa, K., Takezoe, H., and Fukuda, A., *Jpn. J. Appl. Phys.*, *34*, L299 (1995).
77. Debe, M. K., and Kam, K. K., *Thin Solid Films*, *186*, 289 (1990).
78. Debe, M. K., and Poirier, R. J., *Thin Solid Films*, *186*, 327 (1990).
79. Debe, M. K., *J. Vac. Sci. Technol.*, *A4*(3), 273 (1986).
80. Debe, M. K., *J. Appl. Phys.*, *55*(9), 3354, 1984; Erratum: Debe, M. K., and Tommet, T. N., *J. Appl. Phys.*, *62*, 1546 (1987).
81. Abdeldayem, H., Frazier, D. O., Penn, B. G., Witherow, W. K., Banks, C., and Smith, D., *Opti. Communi.* (in press).
82. Casstevens, M. K., Samoc, M., Pfleger, J., and Prasad, P. N., *J. Chem. Phys.*, *92*(3), 2019 (1990).
83. Yariv, A., *Quantum Electronics*, 2nd ed., Wiley, New York, 1975.
84. Hercher, M., *Appl. Opt.*, *6S*(5), 947 (1967).
85. Bloor, D., and Chance, R. R. (eds.), *Polydiacetylenes*, Martinus Nijhoff, Dordrecht, 1985.
86. Chemla, D. S., and Zyss, J., (eds.), *Nonlinear Optical Properties of Organic Molecules and Crystals*, 2, Academic Press., Orlando, FL, 1987.
87. Prasad, P. N., and Williams, D. J., *Introduction to Nonlinear Optical Effects in Molecules and Polymers*, John Wiley & Sons, New York, 1991; especially p. 232.
88. Carter, G. M., Thakur, M. K., Chen, Y. J., and Hryniewicz, J. V., *Appl. Phys. Lett.*, *47*, 457 (1985).
89. Hermann, J. P., and Smith, P. W., in *Digest of Technical Papers—11th International Quantum Electronics Conference*, 1980, p. 656.
90. Paley, M. S., Frazier, D. O., Abdeldeyem, H. A., and McManus S. P., *Chem. Mater.*, *6*(12), 2213 (1994).
91. Tsiboulkis, J., Werninck, A. R., Shand, A. J., and Milburn, G. H. W., *Liq. Cryst.*, *3*(10), 1393 (1988).
92. Kim, T., Crooks, R. M., Tsen, M., and J. Sun, *Am. Chem. Soc.*, *117*, 3963 (1995).
93. Cheong, D. W., Kim, W. H., Samuelson, L. A., Kumar J., and Tripathy, S. K., *Macromolecules*, *29*, 1416 (1996).
94. Kim, W. H., Bihari, B., Moody, R., Kodali, N. B., Kumar, J., and Tripathy, S. K., *Macromolecules*, *28*, 642 (1995).
95. Sandman, D. J., (ed.), *Solid State Polymerization*, American Chemical Society, Washington, DC, 1987.
96. Thakur, M., and Meyler, S., *Macromolecules*, *18*, 2341 (1985).
97. Frazier, D. O., Hung, R. J., Paley, M. S., Penn, B. G., and Long, Y. T., *J. Crystal Growth*, *171*, 288 (1997).
98. Zugrav, M., (personal communication).
99. Reid, R. C., Prausnitz, J. M., and Poling, B. E., *The Properties of Gases and Liquids* 4th ed., McGraw-Hill Book Company (1987).
100. Markham, B. L., Greenwell, D. W., and Rosenberger, F., *J. Crystal Growth*, *51*, 426 (1981).
101. Paley, M. S., Frazier, D. O., McManus, S. P., Zutaut, S. E., and Snagahadasa, M., *Chem. Mater.*, *5*(11), 1641 (1993).
102. Horner, C. J., and Garito, A. F., *Makromol. Chem.*, *182*, 19 (1981).
103. Garito, A. F., Singer, K. D., and Teng, C. C., in *Nonlinear Optical Properties of Organic and Polymeric Materials* (D. J. Williams ed.), ACS Symposium Series 233, American Chemical Society, Washington, DC, 1983, p. 1.
104. Etemad, S., Baker, G. L., and Soos, Z. G., in *Molecular Nonlinear Optics* (J. Zyss, ed.), Academic Press, San Diego, CA 1993.
105. Thakur, M., and Krol, D. M., *Appl. Phys. Lett.*, *56*(13), 1213 (1990).
106. Samoc, M. (personal communication).

107. Stegeman, G. I., Torruellas, W., in *Electrical, Optical, and Magnetic Properties of Organic Solid State Material* (A. F. Garito, A. K. Jen, C. Y-C. Lee, and L. Dalton, eds.), MRS Symposium Proceedings, Materials Research Society, Pittsburgh, 1994, p. 397.
108. Walter, H. U., (ed.), *Fluid Sciences and Materials in Space (ESA)*, Springer-Verlag, New York, 1987.
109. Antar, B., and Nuotio-Antar, V. S., *Fundamentals of Low-Gravity Fluid Dynamics and Heat Transfer*, CRC Press, Boca Raton, FL, 1994.
110. Frazier, D. O., Hung, R. J., Paley, M. S., and Long, Y. T., *J. Crystal Growth, 173*, 172 (1997).
111. Antar, B. N., *Phys. Fluids, 30*(2), 322 (1987).
112. Maxwell Garnett, J. C., *Phil. Trans. Roy. Soc. London 203*, 385 (1904); *205*, 237 (1906).
113. Ricard, D., Rousignol, P., and Flytzanis, C., *Opt. Lett., 10*, 511 (1985).
114. Sipe, J. W., and Boyd, R. W., *Phys. Rev. A46*, 1614 (1992).
115. Brust, M., Walker, M., Bethell, D., Schiffrin, D. J., and Whyman, R., *J. Chem. Soc. Chem. Commun.*, 801 (1994).
116. Paley, M. S, Armstrong, S., Witherow, W. K., and Frazier, D. O., *Chem. Mater., 8*(4), 912 (1996).
117. Bromberg, J. P., *Physical Chemistry*, Allyn and Bacon, Boston, MA, 824, (1980).
118. Dorsinville, R., Yang, L., Alfano, R. R., Zamboni, R., Danieli, R., Ruani, G., and Taliani, C., *Opt. Lett., 14*(23), 1321 (1989).
119. Logsdon, P. B., Pfleger, J., and Prasad, P. N., *Synth. Met., 26*, 369 (1988).
120. Erhardt, J., *Galvanotechnik, 72*(1), 13 (1981).
121. Naumann, R. J., *Microgravity Sci. Tehcnol., VIII/4*, 204 (1995).
122. Riley, C., Coble, H. D., Loo, B., Benson, B., Abi-Akar, H., and Maybee, G., Polym. Prepri., *28*(2), 470 (1987).
123. Riley, C., Coble, D., and Maybee, G., AIAA Paper 87-0510 (1987).
124. Riley, C., Abi-Akar, H., and Benson, B., *J. Spacecraft Rockets, 27*(4), 386 (1990).
125. Dalton, L., et al., *Adv. Mater., 7*, 519 (1995); *Chem. Mater., 7*, 1060 (1995); *Appl. Phys. Lett., 67*, 1806 (1995).
126. Marder, S. R., Perry, J., Staehelin, M., and Zysset, B., *Science, 271*, 335 (1996).
127. Aitchison, J. S., Kean, A. H., Ironside, C. N., Villeneuve, A., and Stegeman, G. I., *Electron. Lett., 28*, 1709 (1991).
128. Villeneuve, A., Yang, C. C., Wigley, P. G. J., Stegeman, G. I., Aitchison, J. S., and Ironside, C. N., *Appl. Phys. Lett., 61*, 147 (1992).
129. Al-hemyari, A., Aitchison, J. S., Ironside, C. N., Kennedy, G. T., Grant, R. S., and Sibbett, W., *Electron. Lett., 27*, 1090 (1992).
130. Atichison, J. S., Villeneuve, A., and Stegeman, G. I., *Opt. Lett., 18*, 1153 (1993).
131. Yang, C. C., Villeneuve, A., Stetgeman, G. I., and Aitchison, J. S., *Opt. Lett., 17*, 710 (1992).
132. Al-hemyari, A., Villeneuve, A., Kang, J. U., Aitchison, J. S., Ironside, C. N., and Stegeman, G. I., *Appl. Phys. Lett., 63*, 3562 (1993).
133. Lee, S. G., McGinnis, B. P., Jin, R., Yumoto, J., Khitrova, G., Gibbs, H. M., Binder, R., Koch, S. W., and Peyghambarian, N., *Appl. Phys. Lett., 64*, 454 (1994).
134. Townsend, P. D., Jackel, J. L., Baker, G. L., Shelburne, J. A., and Eternad, S., *Appl. Phys. Lett., 55*, 1829 (1989).
135. Rochford, K. B., Zanoni, R., Gong, Q., and Stegeman, G. I., *Appl. Phys. Lett., 55*, 1161 (1989).
136. Kim, D. Y., Lawrence, B. L., Torroellas, W. E., Stegeman, G. I., Baker, G., and Meth, J., *Appl. Phys. Lett., 65*, 1742 (1994).